Lateral Torsional Buckling Resistance of Horizontally Curved Steel I-Girders

by

Nolan James Rettie

A thesis submitted in partial fulfillment of the requirements for the degree of

Master of Science
in
Structural Engineering

Department of Civil and Environmental Engineering
University of Alberta

ABSTRACT

The current design provisions (2006 edition of CSA-S6) for horizontally curved steel I-girders in the Canadian Highway Bridge Design Code are based on research conducted prior to the mid 1980's. Much research, experimental and numerical analysis, on horizontally curved girders has been conducted over the past 30 years. A review of the available data was conducted and areas where more information is required were identified. Although extensive research has been conducted on horizontally curved I-girders, there were limited experimental and numerical results on girders with flanges that were Class 3 or better that failed below 80% of the beam's yield moment. Elastic and inelastic lateral torsional buckling failures typically occur below 80% of the beam's yield moment.

A parametric study was conducted, focusing on lateral torsional buckling behaviour of horizontally curved girders. The parametric study included a total of 36 single horizontally curved girder models that varied the following parameters: the radius of curvature, the flange width-to-thickness ratio, and the web height-to-thickness ratio. The parametric study was conducted using finite element analysis. The development of the finite element models included validating the models by comparing with previous experimental and numerical results. Different curved girder design equations were explored, and three were chosen to be investigated. They were compared based on the actual moment resistances found from the models to determine which equation performed best. Based on the analysis results, the proposed equation for the 2014 edition of CSA-S6 best predicts the actual moment resistance for curved girders. The mean calculated-to-actual moment resistance ratio was 0.90 and the coefficient of variation was 0.10 for first-order analyses, 0.98 and 0.08 respectively, for second-order analyses.

To EUPA, for teaching me the meaning of Community.

ACKNOWLEDGEMENTS

A number of individuals need to be thanked for their support to the overall success of this project. First, the author wishes to thank Dr. Gilbert Grondin and Dr. Marwan El-Rich, his supervisors, for their guidance throughout the project. Charles Albert from the Canadian Institute of Steel Construction is also recognized for providing additional model information for the curved bridge design example. Discussions, advice and venting sessions with Kristin Thomas and Graeme Johnston have also been vital to the completion of this work.

The author wishes to thank his family Don, Jana, Denise, Bryce, and Danielle for their constant support. His Edmonton family, Barb, Gary, Todd, Kayley, Leah, and Abbey are also acknowledged for providing additional motivation to finish this work. Finally, I would like to thank Em for her support, encouragement, understanding, and patience through all of this.

Financial support for the research was provided by the Natural Sciences and Engineering Research Council of Canada, and Stantec Consulting. The support and encouragement of my colleagues at Stantec was extremely helpful during these last months.

TABLE OF CONTENTS

LIST OF TABLES

LIST OF FIGURES

LIST OF SYMBOLS

A	=	amplification factor
A_w	=	cross-sectional area of the weld metal
a	=	stiffener spacing
b	=	flange width
b_{fc}	=	width of the compression flange
C_b	=	moment gradient modifier
c_f	=	tension block width due to flame-cutting alone
c_{fw}	=	final tension block width, including flame-cutting and welding
c_w	=	tension block width due to welding alone
$[DAF]_{vm}$	=	deflection amplification factor for von Mises stress, can be taken conservatively as 3.0
E	=	modulus of elasticity
F_b	=	allowable stress due to vertical bending
F_{bc}	=	allowable bending stress in curved beam
F_{bs}	=	allowable bending stress in straight beam
F_{cr}	=	elastic lateral torsional buckling stress
F_n	=	nominal flexural resistance for a straight beam
F_{nc}	=	nominal flexure resistance of the flange
F_w	=	normal stress due to lateral flange bending or warping
F_y	=	yield strength of the plate
F_{yc}	=	yield strength of compression flange
F_{yr}	=	yield stress including residual stress effects
f_b	=	vertical bending stress
f_{bu}	=	major axis bending stress

f_l	=	lateral bending stress
f_w	=	co-existing warping normal stress
h	=	web height
h_c	=	height of the web compression zone
L	=	unsupported length of compression flange
L_b	=	unbraced length
L_p	=	limiting unbraced length to achieve nominal flexural resistance of the cross-section
L_r	=	limiting unbraced length to achieve onset of nominal yielding in either flange under uniform bending with consideration for residual stress effects
M_{calc}	=	calculated moment resistance
M_{fw}	=	factored bending moment in the flange due to warping
M_{fx}	=	factored moment about the strong axis
M_p	=	plastic moment
M_r	=	moment resistance
M_{rx}	=	moment resistance about the strong axis
M'_{rx}	=	moment resistance for a curved girder to meet stability requirements
M_{ry}	=	moment resistance about the weak axis
M_u	=	elastic lateral torsional buckling moment resistance
M_y	=	yield moment
p	=	welding process efficiency factor
R	=	radius of curvature
R_b	=	web load-shedding factor
R_h	=	hybrid factor
r_t	=	effective radius of gyration for lateral torsional buckling
S_x	=	elastic section modulus about the major axis

S_y	=	elastic section modulus about the weak axis
t	=	flange thickness, or plate thickness in residual stress calculations
t_{fc}	=	thickness of the compression flange
t_w	=	web thickness
U_c	=	amplification factor
w	=	web thickness
w_c	=	0.5 when lateral bending moment in the flange has major reversals, equal to 1.0 otherwise
x	=	subtended angle between vertical supports, equal to the span length divided by the radius of curvature
y	=	critical moment ratio
α	=	empirical constant equal to 2.152
β	=	empirical constant equal to 2.129
β_1	=	constant based on location of moment, conservatively taken as 0.0667
γ	=	empirical constant equal to 0.1058
ε_{eng}	=	engineering strain
ε_{true}	=	true strain
λ	=	slenderness of laterally unsupported segment
λ_f	=	slenderness ratio for the compression flange
λ_{pf}	=	limiting slenderness ratio for a compact flange
λ_{rf}	=	limiting slenderness ratio for a non-compact flange
ν	=	Poisson's ratio
ρ_b	=	bending stress, or horizontal curvature correction factor
ρ_w	=	lateral flange bending stress, or warping stress correction factor
Σt	=	sum of the plate thicknesses meeting at the weld
σ_b	=	bending stress

σ_c = compressive residual stress

σ_{eng} = engineering stress

σ_{true} = true stress

σ_w = warping stress

ϕ_f = resistance factor for flexure

ϕ_s = resistance factor for steel

Ψ_w = factor for curvature effects on maximum stresses in web panel

ω_2 = moment gradient factor

CHAPTER 1

INTRODUCTION

1.1 Statement of the Problem

Horizontally curved steel I-girder highway bridges have seen a significant increase in popularity over the past 30 years because of the demand placed on highway structures by the roadway alignment and tight geometric restrictions required to maintain safe traffic design speeds. As more emphasis is placed on aesthetics and analysis software and hardware become more readily available in the design office, bridge designers are in greater need for guidance. The American Association of State Highway and Transportation Officials (AASHTO) first published the Guide Specifications for Horizontally Curved Girder Highway Bridges in 1980. Since then, there has been a large volume of research, both experimental and numerical, to provide a better understanding of the strength and behaviour and more accurate prediction of the capacity of horizontally curved bridges.

The analysis, design and construction of horizontally curved girder bridges are quite difficult. Because of the horizontal curvature, the girders are subjected to bending and torsion when loaded vertically. Due to the differing horizontal and vertical displacements between adjacent curved girders, there is an increased interaction between girders connected with cross-frames. Therefore, cross-frames are considered primary structural members in a curved girder bridge system. The increased interaction between girders and bracing and the general behaviour of horizontally curved members increases the complexity of the behaviour of considerably.

Although there has been extensive research done into the behaviour of horizontally curved steel I-girders, there were limited experimental and numerical results on girders with flanges that were Class 3 or better that failed below 80% of their yield moment. Elastic and inelastic lateral torsional buckling (LTB) failures typically occur below 80% of the beam's yield moment.

AASHTO adopted new design provisions for horizontally curved girders in their bridge specifications in 2006. This was based on research conducted since 1980. The Canadian Highway Bridge Design Code (CHBDC) design provisions have not been updated recently, and the horizontally curved girder design equations are currently based on research conducted prior to 1980.

1.2 Objectives and Scope

There is a large body of test and analysis results on horizontally curved girders. This research project was initiated to collect and critically assess the available data and identify areas where more information is required. A parametric study will be conducted to expand the research database where needs are identified. This parametric study includes a total of 36 single girder models where the following characteristics were varied: the radius of curvature, the flange width-to-thickness ratio, and the web height-to-thickness ratio. The parametric study will focus on studying the lateral torsional buckling behaviour of horizontally curved girders. Possible curved girder design equations will be assessed and a recommendation for use by bridge engineers will be made.

1.3 Organization of Thesis

This thesis consists of five chapters. Chapter 2 contains a literature review on flexural behaviour of horizontally curved steel members. Capacity equations developed for curved girder design, as well as an overview of the design standards used in Canada and the United States. Development and validation of a finite element model of horizontally curved girders is discussed in Chapter 3. Details of mesh discretization, material properties, loading conditions, boundary conditions, residual stress effects, analysis method, and details of validation with previous research are provided. Chapter 4 outlines the parametric study that was conducted to expand the database of analysis results in an area where a lack of information was identified. Finally, a summary of the research is presented in Chapter 5 and conclusions about the design and behaviour of horizontally curved steel I-girders are made, as well as recommendations for future research. Appendix A includes sample calculations for the capacity equations that were investigated, as well as parameters that were used for the finite element model such as, residual stresses and end span lengths.

CHAPTER 2

LITERATURE REVIEW

2.1 Overview

A review of the current available research on horizontally curved girders will be presented. The history of the development of available design guides and standards is discussed, followed by an overview of various experimental testing a numerical modeling programs. Various design equations that have been developed will be described, followed by the current equations used by the American Association of State Highway and Transportation Officials (AASHTO) and the Canadian Standards Association (CSA). Finally, an area for further research is identified in order to provide a recommendation for a design equation to be used in bridge design standards.

2.2 Development of Design Standards

In 1969 the Federal Highway Administration (FHWA) created the Consortium of University Research Teams (CURT) project. The CURT project consisted of research teams from various universities sponsored by 25 participating state highway departments, whose main objective was to assemble a comprehensive review of all the published information on curved girders. The efforts of the CURT project resulted in the publications of working stress design criteria and tentative design specifications for curved bridges. In 1976 the American Society of Civil Engineers (ASCE) and AASHTO compiled all up to date research and created a set of recommendations related to the design of curved I-girder bridges. The first *Guide Specifications for Horizontally Curved Highway Bridges* (hereafter referred to as the "Guide Specifications") was published in 1980 (AASHTO 1980). The 1980 Guide Specifications were presented in Allowable Stress Design (ASD) format. An updated version of the Guide Specifications was published in 1993 (AASHTO 1993). It included both ASD and Load and Resistance Factor Design (LRFD) provisions.

The 1993 Guide Specifications were based on research performed through the CURT project done in the early 1970s and had significant deficiencies, resulting mainly from the

limited knowledge about horizontally curved girders at the time the design guide was published (NCHRP 1999). The National Cooperative Highway Research Program (NCHRP) funded project 12-38 in the early 1990s. The objective of project 12-38 was to develop a revised design specification for horizontally curved girders. These specifications were to be based on current design practice and technology. They were to be used as a recommendation to AASHTO for adoption. One of the tasks associated with NCHRP Project 12-38 was to develop a "unified" design approach that could be applied to straight and horizontally curved girders. An updated version of the Guide Specifications was published by AASHTO in 2003 based on the recommendations provided by Project 12-38 (NCHRP 2006).

After NCHRP project 12-38, the body of knowledge on horizontally curved bridges was deemed sufficient to incorporate design provisions for horizontally curved bridges into the AASHTO *LRFD Bridge Design Specifications.* In 1999, the NCHRP funded project 12-52 to develop curved bridge design provisions for AASHTO in LRFD format (NCHRP 2006). The horizontally curved bridge provisions were included in the 2006 interim to the AASHTO *LRFD Bridge Design Specifications, 3rd Edition* (NCHRP 2006). The Curved Steel Bridge Research Project (CSBRP) was also initiated in the early 1990s. The research results and design equations developed from the CSBRP were included in the recommendations from NCHRP project 12-52.

When the Guide Specifications were developed there was only one other design specification for curved steel girders. The *Guidelines for the Design of Horizontally Curved Girder Bridges* (hereafter referred to as the Hanshin Guidelines), was developed by the Hanshin Expressway Public Corporation in Japan. The Hanshin Guidelines referred to the Japanese Road Association Specifications for Highway Bridges for the basic requirements and it contained mainly provisions that were directly influenced by the effects of curvature. The guidelines were presented in allowable stress design format.

2.3 Experimental Programs

Previous experimental research programs on horizontally curved girders are described in the following sections.

2.3.1 Mozer and Culver (1970); Mozer et al. (1971), (1973)

A series of tests were conducted on horizontally curved girders as part of the CURT project. The tests were designed to determine the ultimate capacity of curved girders under bending, shear, and combined bending and shear. All specimen cross-sections were doubly-symmetric.

The first series of tests, P1, consisted of seven, single-girder test specimens used for one or two ultimate load tests (Mozer and Culver 1970). The distinct failure modes observed were local buckling of the compression flange and shear failure of the web panel. The authors concluded that the flange slenderness limits for straight girders can be conservatively used for horizontally curved girders, if the flanges were cut-curved.

The second series of tests, P2, consisted of six tests on two curved girders (Mozer *et al.* 1971). Three separate loading conditions, tests A, B and C, were conducted on each specimen. Test A was a four-point bending test. The purpose was to determine the bending resistance under constant moment, for different lateral support stiffness at the load points. The flexibility of the lateral supports was found to have negligible effect on the resistance. Tests B and C on the first test specimen were designed to cause shear failure in the web panels adjacent to the applied load. Tests B and C on the second test specimen were intended to create combined shear and flexural failure. Flexural failure was initiated by local buckling of the compression flange. The bending failure modes were difficult to distinguish between local buckling, section capacity or lateral torsional buckling. This was due to the gradual increase in lateral displacements associated with horizontally curved beams loaded vertically. It was difficult to identify a point of equilibrium bifurcation. The results of these tests supported the conclusions developed from the P1 series and that adequately braced compression flanges can develop significant post-yield bending capacity.

The third series of tests, P3, consisted of eight tests on pairs of girders connected by diaphragms (Mozer *et al.* 1973). The testing program was designed to explore the bending strength of horizontally curved plate girders in a multi-girder bridge system, strength and behaviour of web plates in curved girders, and the influence of transverse stiffeners on web strength. As stated previously, lateral torsional buckling is difficult to identify in curved girders, however it is unlikely to have been a failure mode because all

test specimens obtained at least 96% of their full-plastic moment. The authors concluded that cross-frames significantly affect the behaviour of curved I-girder bridge system.

The research conducted through the CURT project consisted of girder dimensions that are not typical for highway bridge design. All specimens were less than 500 mm deep and span lengths were less than 6 m.

2.3.2 Nakai and Kotoguchi (1983)

The Hanshin Expressway Public Corporation developed a design guideline for curved girder bridges (Nakai and Yoo 1988), partially based on 27 tests on single girders under constant moment conducted by Nakai and Kotoguchi (1983). These tests were conducted on girders of spans, from 0.9 m to 2.5 m. Information on girder web and flange dimensions, as well as end restraint conditions, was not found. This lack of information made it difficult to interpret what failure modes were observed during testing.

2.3.3 Shanmugam et al. (1995)

Ten horizontally curved beams were tested by Shanmugam *et al.* (1995). The cross-section dimensions were the same for all specimens. The varied parameters were the fabrication process and the radius of curvature. The vertical supports were between 3.0 m and 5.0 m apart, and lateral supports were provided at the span quarter points, where the point loads were applied. Seven specimens were hot-rolled then cold bent to the specified curvature. Three specimens were built-up from welded plates that were then cold bent to the specified curvature.

Shanmugam *et al.* (1995) reported that all beams failed by lateral torsional buckling and experienced a reduction in ultimate capacity due to horizontal curvature. The reduction in capacity was more significant in the welded sections; Shanmugam *et al.* (1995) suggested that this reduction in capacity was the result of residual stresses.

The testing conducted by Shanmugam *et al.* (1995) consisted of girder dimensions that are not typical for highway bridge design. All specimens were 305 mm in depth and span lengths were less than 5.4 m.

2.3.4 Hartmann (2005)

As part of the CSBRP, a series of tests using a full-scale, horizontally curved, 3-girder, non-composite test frame was conducted (Hartmann 2005). The test specimens consisted of a removable segment of the test frame as shown in Figure 2-1 between the two splices of the exterior girder (girder G3). The specimens were designed and tested to investigate flexural failure. The permanent test-frame members were oversized to ensure that they remained elastic during the flexural failure of the removable test specimens. Neglecting the self-weight of the test-frame, a uniform bending moment distribution was created by six equal point loads that loaded all three girders. Each test specimen would reach a peak applied moment, M_r, during, the loading. After reaching this applied moment, the vertical load continued to increase while the moment in the test specimen decreased as more of the load would be shed to the other girders. This peak moment resistance was reported as the flexural capacity of the test specimen. The moment in the test specimen was measured using moment equilibrium on a free-body diagram with a section-cut through all three girders in the middle of the span. Strain gauges on the permanent girders that remained elastic, provided the moment in the two girders. These moments, combined with the support reactions and the applied point loads, allowed the moment in the test specimen to be calculated.

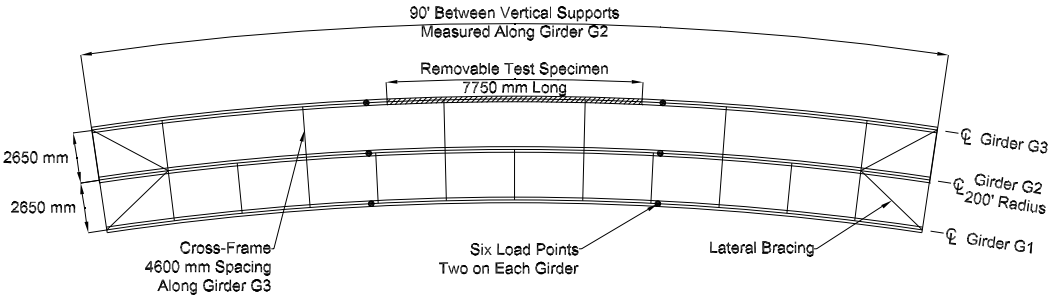

Figure 2-1: Non-composite test frame (Hartmann 2005)

The results of the tests by Hartmann (2005) are shown in Table 2-1. All specimens were welded sections with the flanges cut to the desired radius. All specimens had a constant length and radius as shown in Figure 2-1. They were all fabricated from A572 Grade 50 steel with a nominal yield strength of 345 MPa. Specimens B4 and B7 were monosymmetric sections while all other specimens were doubly symmetric. The yield moment, M_y, of each section was calculated as shown in Table 2-1.

Table 2-1: Non-composite test frame data (Hartmann 2005)

ID	Compression Flange		Tension Flange		Web		Flange Class			
	b (mm)	t (mm)	b (mm)	t (mm)	h (mm)	w (mm)		M_r (kN·m)	M_y (kN·m)	$\frac{M_r}{M_y}$
B1	444	19.5	445	19.4	1211	8.2	4	4539	4945	0.91
B2	443	19.4	443	19.4	1212	10.1	4	4730	5092	0.93
B3	443	19.5	445	19.4	1213	10.2	4	4834	5147	0.94
B4	443	19.4	533	32.4	1212	8.1	4	4880	5269	0.93
B5	419	24.7	420	24.6	1215	8.5	2	5278	5764	0.92
B6	414	30.9	414	31.0	1214	8.6	1	6400	6817	0.94
B7	533	16.4	445	19.2	1215	8.4	4	3503	3531	0.99

Instability governed the ultimate capacity of all the specimens. The reported failure modes were flange local buckling for the specimens with a Class 4 flange, and lateral torsional buckling for specimens B5 and B6. All specimens achieved a moment resistance of at least 92% of the yield moment.

2.3.5 Jung (2006)

The last phase of the CSBRP included testing of a full-scale, composite, multi-curved-girder test specimen (Jung 2006). The test specimen was designed in accordance with AASHTO *LRFD Bridge Design Specifications, 3rd Edition*. The test configuration was a simply-supported single span, and the compression flange of the girders was continuously supported laterally by the concrete deck. The composite bridge had three girder lines, G1, G2 and G3. Three intermediate cross-frames were used to connect the girders between the vertical supports. The radius of curvature increased from G1 to G3. The composite bridge configuration is shown in Figure 2-2. The test geometry did not change, but the loading configuration was varied.

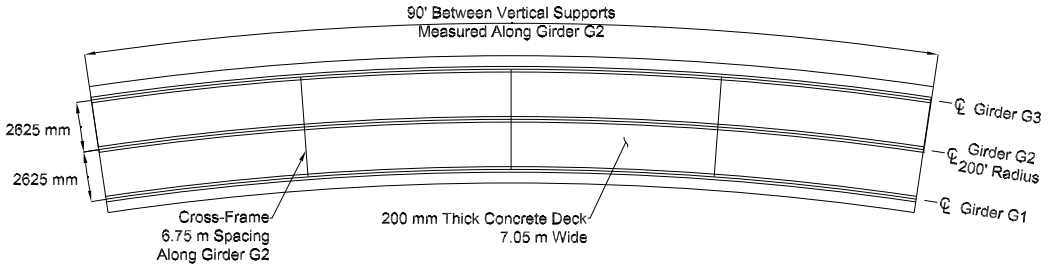

Figure 2-2: Composite test bridge (Jung 2006)

Four tests were conducted on the composite girders. Test 1 addressed the generation of influence surfaces by applying a 72 kN concentrated load at different grid points on the slab. Tests 2 and 3 consisted of loading the test bridge with a group of six loads applied by hydraulic jacks directly above the girders. For Test 2 the loads were applied directly above girders G2 and G3, creating maximum moments in G3. In Test 3 the loads were applied above G1 and G2, creating maximum flexural effects in G1. Tests 4a and 4b, were designed to simulate the equivalent of two AASHTO design trucks plus two lane loads. This was achieved by applying load using a group of nine hydraulic jacks. Test 4a involved two repeated loading sequences at several load levels defined in relation to various design limits (AASHTO 2004) and other limits. Test 4b, was the final test, and the only test that loaded the test bridge to its ultimate capacity. The ultimate capacity in the test bridge was reached when spalling and crushing of the concrete deck occurred, which was after the steel girders had reached their plastic moment. Although lateral torsional buckling was not observed in the test bridge, the FEA study developed from the test bridge, modified the end conditions to simulate a continuous bridge, thus resulting in failure of girder G1 by lateral torsional buckling. The FEA study is discussed further in Section 2.4.2.

From the experimental tests and following numerical analyses the author concluded that the a girder section's plastic moment, M_p, can be used when designing curved girders that meet the compact section requirements stated in AASHTO's bridge design code. Previously, the design of curved girder sections was limited to their elastic moment for design, even if they met the compact section requirements.

2.4 Numerical Analyses

Previous research programs on horizontally curved girders utilizing finite element analysis (FEA) are described in the following sections.

2.4.1 Davidson (1992)

Davidson (1992) conducted an extensive parametric study to investigate the lateral torsional buckling and local buckling resistance of horizontally curved girders. The majority of these models were in the elastic region of the lateral torsional buckling curve, with buckling failure occurring at 33% of the yield moment or lower. Some FEA

buckling failure moments were between 60 and 70 percent of the yield moment. However, these models used girders with web depths of 450 mm or less, and web slenderness, h/w, ratios of 40 or less, which are not typical dimensions for highway bridges.

The author concluded that the nominal shear strength for a straight panel that included tension field action, be used for that of the curved girder (Davidson 1992). Under pure bending, the nonlinear transverse "bulging" displacement behaviour reduces the moment carrying capacity of the curved section, compared to the straight section. The "lateral pressure analogy" described in Section 2.5.3 was used to develop Equation 2.3.

These analysis results were not compared with experimental results. Straight girders were modeled and the results of analyses on straight girders were compared with theoretical strengths to validate the modeling and analysis procedures. The horizontally curved girder capacities were then compared to the equivalent straight girders, of the same length and cross-section.

2.4.2 White et al. (2001)

White *et al.* (2001) conducted a parametric study as part of the CSBRP project to develop unified design equations for curved and straight I-girders. Finite element models were developed and validated with the test results from Hartmann (2005). These models accounted for initial geometric imperfections, nonlinear and inelastic material behaviour, support conditions and residual stresses. The parametric study was designed to represent a wide range of practical girder geometries and boundary conditions. It was subdivided into six groups of analysis. Single girder models were used for all analysis groups.

The primary group of finite element models was designed to evaluate the behaviour of I-girders under uniform vertical bending moment, maximum shear-to-moment ratio, and combination of high shear and high moment. The primary group served as a basis for the other test groups. The modified uniform vertical bending group was designed to determine the effect of radial displacement of the compression flange at cross-frame locations. This was done by applying an outward radial displacement to the top flange at the radial support locations. Another loading group was developed to determine the effect of load height on curved girders. All of the previous bending groups discussed consider

an internal girder segment, the free-end group was created to study the behaviour of curved girders at the bridge ends.

All test groups discussed thus far used doubly symmetric cross-sections. The behaviour of monosymmetric girders was also investigated. A group of laterally unsupported straight girder was designed to develop unified equations for curved and straight girders. The web depth and yield strength remained constant at 1219 mm and 345 MPa, respectively. The curved girder study varied six parameters, namely, the web height-to-flange width ratio, h/b, the flange slenderness ratio, b/t , the web slenderness ratio, h/w, the stiffener spacing-to-web-height ratio, a/h, the unbraced length-to-radius of curvature ratio, L_b/R, and the lateral bending stress-to-vertical bending stress ratio, f_l/f_b. The specimens included in the parametric study were designated with a six-number label. The numbers in the label correspond to the value of each non-dimensional parameter as follows:

$$h/b - b/t - h/w - a/h - L_b/R - f_l/f_b$$

where h = web height
b = flange width
t = flange thickness
w = web thickness
a = stiffener spacing
L_b = unbraced length
R = radius of curvature
f_l = target elastic lateral bending stress
f_b = target elastic vertical bending stress

There were 138 models subjected to a uniform bending moment. Of those 138, only 58 models used Class 3 or better girder flanges. These models are shown in Table 2-2. Column 4 shows the moment resistance determined from the finite element analysis, M_r. Column 5 shows the calculated yield moment of the section, M_y. Column 6 shows the ratio of moment resistance to yield moment ratio, M_r/M_y. All models experienced flexural failures, but it was difficult to distinguish between local flange buckling and lateral torsional buckling.

Table 2-2: Non-composite parametric study (White *et al.* 2001)

Model #	Model ID	Flange Class			
	b/t - h/w - a/h - L_b/R - f_l/f_b		M_r (kN·m)	M_y (kN·m)	$\frac{M_r}{M_y}$
(1)	(2)	(3)	(4)	(5)	(6)
1	2.75-20-160-2-0.050-0.50	3	3862	4768	0.81
2	2.75-20-160-3-0.050-0.50	3	3862	4768	0.81
3	2.75-15-160-3-0.050-0.50	1	5027	6131	0.82
4	2.75-20-100-3-0.050-0.50	3	4219	5145	0.82
5	2.75-20-130-3-0.050-0.50	3	4029	4913	0.82
6	2.75-15-130-3-0.050-0.50	1	5208	6274	0.83
7	2.75-20-160-1-0.050-0.50	3	3957	4768	0.83
8	2.75-15-160-1-0.050-0.50	1	5150	6131	0.84
9	2.75-15-160-2-0.050-0.50	1	5150	6131	0.84
10	2.75-15-100-3-0.050-0.50	1	5529	6504	0.85
11	2.75-20-160-3-0.050-0.35	3	4053	4768	0.85
12	2.75-20-160-3-0.100-0.50	3	4053	4768	0.85
13	2.75-20-160-2-0.100-0.50	3	4100	4768	0.86
14	2.75-15-160-2-0.100-0.35	1	5334	6131	0.87
15	2.75-15-160-3-0.075-0.50	1	5334	6131	0.87
16	2.75-15-160-3-0.100-0.50	1	5334	6131	0.87
17	2.75-20-130-3-0.100-0.50	3	4274	4913	0.87
18	2.75-20-160-1-0.100-0.50	3	4148	4768	0.87
19	2.75-15-160-1-0.100-0.35	1	5395	6131	0.88
20	2.75-15-160-1-0.100-0.50	1	5395	6131	0.88
21	2.75-15-160-2-0.075-0.50	1	5395	6131	0.88
22	2.75-15-160-2-0.100-0.50	1	5395	6131	0.88
23	2.75-15-160-3-0.075-0.35	1	5395	6131	0.88
24	2.75-20-100-3-0.100-0.50	3	4528	5145	0.88
25	2.75-20-130-3-0.050-0.35	3	4323	4913	0.88
26	2.75-20-160-2-0.075-0.50	3	4196	4768	0.88
27	2.75-20-160-3-0.075-0.35	3	4196	4768	0.88
28	2.75-20-160-3-0.075-0.50	3	4196	4768	0.88
29	2.75-15-130-3-0.100-0.50	1	5584	6274	0.89
30	2.75-15-160-2-0.075-0.35	1	5457	6131	0.89
31	2.75-20-130-3-0.075-0.50	3	4372	4913	0.89
32	2.75-20-160-1-0.050-0.35	3	4243	4768	0.89
33	2.75-20-160-1-0.075-0.50	3	4243	4768	0.89
34	2.75-20-160-2-0.050-0.35	3	4243	4768	0.89
35	2.75-20-160-2-0.075-0.35	3	4243	4768	0.89
36	2.75-15-130-3-0.075-0.50	1	5647	6274	0.90
37	2.75-15-160-1-0.075-0.35	1	5518	6131	0.90
38	2.75-15-160-3-0.050-0.35	1	5518	6131	0.90
39	2.75-20-100-3-0.050-0.35	3	4631	5145	0.90
40	2.75-20-160-1-0.075-0.35	3	4291	4768	0.90
41	2.75-20-160-2-0.100-0.35	3	4291	4768	0.90
42	2.75-15-100-3-0.100-0.50	1	5919	6504	0.91

Table 2-2 (Cont'd): Non-composite parametric study (White *et al.* 2001)

Model #	Model ID	Flange Class			
	b/t - h/w - a/h - L_b/R - f_l/f_b		M_r (kN·m)	M_y (kN·m)	$\frac{M_r}{M_y}$
(1)	(2)	(3)	(4)	(5)	(6)
43	2.75-15-160-1-0.075-0.50	1	5579	6131	0.91
44	2.75-20-100-3-0.075-0.50	3	4682	5145	0.91
45	2.75-20-130-2-0.100-0.35	3	4471	4913	0.91
46	2.75-20-130-3-0.075-0.35	3	4471	4913	0.91
47	2.75-20-160-1-0.100-0.35	3	4339	4768	0.91
48	2.75-15-100-3-0.075-0.50	1	5984	6504	0.92
49	2.75-15-130-2-0.100-0.35	1	5773	6274	0.92
50	2.75-15-130-3-0.050-0.35	1	5773	6274	0.92
51	2.75-15-130-3-0.075-0.35	1	5773	6274	0.92
52	2.75-15-160-2-0.050-0.35	1	5641	6131	0.92
53	2.75-20-100-2-0.100-0.35	3	4734	5145	0.92
54	2.75-15-100-3-0.075-0.35	1	6049	6504	0.93
55	2.75-15-160-1-0.050-0.35	1	5702	6131	0.93
56	2.75-20-100-3-0.075-0.35	3	4785	5145	0.93
57	2.75-15-100-3-0.050-0.35	1	6179	6504	0.95
58	2.75-15-100-2-0.100-0.35	1	6244	6504	0.96

2.4.3 Jung (2006)

A parametric study similar to that conducted by White *et al.* (2001) was conducted by Jung (2006) except that it considered composite bridges. Seven sets of parametric studies were developed from the base finite element model that was validated against measured experimental responses.

The first parametric study explored the effects of using different connection detailing methods. The girders were detailed to have the web plumb either during erection or after the total dead loads were applied. One study was designed to determine the effect of using a hybrid exterior girder, made of steel of various grades. Another study was designed to examine the effect of cross-frame spacing. The effect of cross-frame yielding was examined in another parametric study. A continuous system was created to study the negative moment regions in a composite bridge. The final two studies involved skewed bridges and the addition of a design lane. Further details of all of these studies can be found in Jung (2006).

Only one model from the continuous bridge study failed by a combination of lateral torsional buckling, flange local buckling and web bend buckling (Jung 2006). Because the FEA model was a composite bridge typically subjected to loads that caused positive bending, the lateral torsional buckling resistance of curved girders was not explored.

2.5 Capacity Equations

2.5.1 One-Third Rule

The desire for "unified" resistance equations for curved and straight girder bridges led to the development of the one-third rule. The one-third rule represented by Equation 2.1, accounts for the combined effects of major axis bending and flange lateral bending.

$$f_{bu} + \frac{1}{3} f_l \leq F_n \qquad [2.1]$$

where f_{bu} = major axis bending stress
f_l = lateral bending stress
F_n = nominal flexural resistance for a straight beam

The advantage of a unified equation is that the load side, $f_{bu} + \frac{1}{3} f_l$, and the resistance side of the equation, F_n, are the same for both curved and straight girders. The resistance is calculated using the same equations and failure modes for curved and straight girders. The failure modes include yielding of the cross-section, local buckling of laterally supported members, and elastic or inelastic lateral torsional buckling of laterally unsupported members. Bending about the major axis creates major axis bending stresses, f_{bu}, in the flange. These stresses are uniform across the flange width. When a horizontally curved girder is loaded in the vertical direction, lateral bending stresses, f_l, create warping of the cross-section under the torsional effect introduced by the horizontal curvature of the girder. These stresses vary linearly across the flange width. Since the "unified" equation is used for straight and curved girders $f_l = 0$ for straight girders. The lateral bending and vertical bending stresses are typically determined from numerical analysis.

Referring to Equation 2.1, it is clear that the bending capacity of a curved girder will be lower than that of an equivalent straight girder, due to the additional $\frac{1}{3} f_l$ term on the load

side of the equation. The derivation of the one-third rule is explained in White and Grubb (2005).

2.5.2 Simple Regression Equation

To determine the reduction in critical lateral torsional buckling capacity of curved girders compared to straight girders Yoo *et al.* (1996) proposed Equation 2.2.

$$y=(1-\gamma x^{\beta})^{\alpha} \quad [2.2]$$

where y = critical moment ratio, *i.e.*, ratio of curved to straight girder capacities
γ = empirical constant equal to 0.1058
x = subtended angle between vertical supports, equal to the span length divided by the radius of curvature
β = empirical constant equal to 2.129
α = empirical constant equal to 2.152

The equation was developed from finite element analyses. The finite element model considered two load cases, uniformly distributed load and constant moment. The FEA results showed that the loading condition had negligible effect on the critical moment ratio. As a result, the only variable in Equation 2.2 is the subtended angle, x, which relates the span length to the radius of curvature.

2.5.3 Pressure Vessel Analogy

When horizontally curved girders are loaded vertically they are subjected to a combination of bending about their strong axis and torsion, which gives rise to warping stresses in the flanges. This can be visualized as the effect of the non-collinearity of the normal stresses in the cross-section from major-axis bending (CISC 2011), which tends to force the compression flange to deflect laterally away from the centre of curvature and the tension flange to deflect towards the centre of curvature. A pressure vessel analogy, illustrated in Figure 2-3, relates the effect of the flange force (analogous to the hoop stress in a pressure vessel) to a "virtual radial pressure" (analogous to the internal pressure in a pressure vessel), which causes lateral bending of the flange. The hoop stress is taken as the normal stress in the flange or web resulting from strong axis bending and the virtual radial pressure is obtained from pressure vessel theory. For the compression flange, the virtual radial pressure acts outward from the centre of curvature. This creates a lateral bending moment distribution similar to that of a continuous beam where the cross-frames

and diaphragms act as supports. This will create movement away from the centre of curvature, *i.e.*, bulging of the compression flange and the compression portion of the girder web. Due to this distortion, lateral displacements and stresses will be amplified (Davidson *et al.* 1999a).

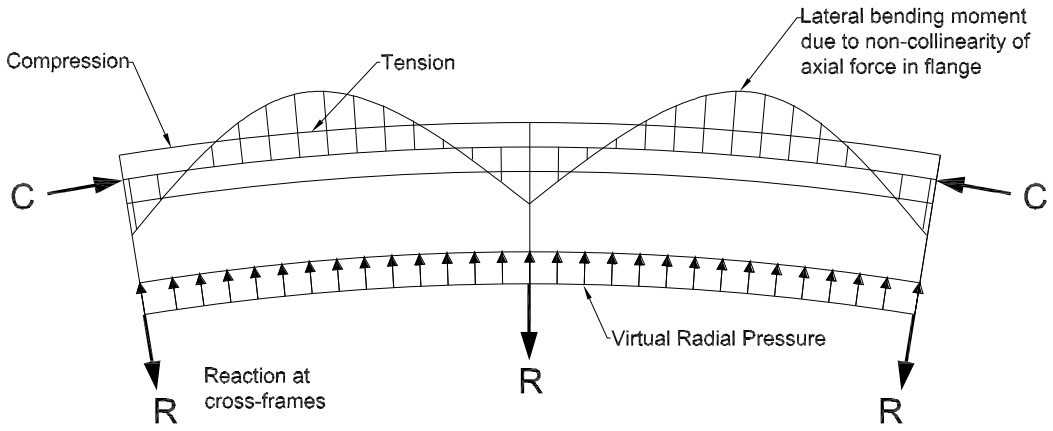

Figure 2-3: Plan view of compression flange of curved I-girder (CISC 2011)

Davidson *et al.* (1999b) found that the elastic web buckling load of a curved panel under pure shear is greater than that for a flat or straight panel. Therefore, they did not develop an equation to predict the critical elastic buckling load for curved girders. However, premature yielding at the flange to web junction due to horizontal curvature should be accounted for. The maximum stress reduction was proposed as:

$$f_b \Psi_w \leq F_b \qquad [2.3]$$

where f_b = calculated stress in compression flange due to vertical bending
Ψ_w = factor for curvature effects on maximum stresses in web panel
F_b = allowable stress due to vertical bending

The factor for curvature is calculated as follows:

$$\Psi_w = \sqrt{1 + \left[\frac{6\beta_1 h_c^2}{t_w R}\right](1\text{-}2\nu) + \left[\frac{6\beta_1 h_c^2}{t_w R}\right]^2 (1\text{-}\nu+\nu^2)\,[DAF]_{vm}} \qquad [2.4]$$

where β_1 = constant based on location of moment, conservatively taken as 0.0667
h_c = height of the web compression zone
t_w = web thickness
ν = Poisson's ratio, 0.3
R = radius of curvature
$[DAF]_{vm}$ = deflection amplification factor for von Mises stress, can be taken conservatively as 3.0

Equations 2.3 and 2.4 were developed based on the theoretical "lateral pressure analogy" but were verified using finite element analysis.

2.5.4 Allowable Stress Curved Column Buckling

The current edition of S6 is based on allowable stress LTB equations developed in the 1970s. The LTB equations are applicable to both symmetric and unsymmetrical girders because lateral torsional buckling is treated as a case of lateral buckling of the compression flange under the combined action of strong axis bending and lateral bending. Local buckling had been known to occur when the combined warping and bending stresses reach the yield strength at the outer edge of the flange tip. Since warping and bending are linearly related, McManus (1971) found that the non-dimensional initial yield moment could be expressed as:

$$M/M_y = 1/(1+\sigma_w/\sigma_b) \qquad [2.5]$$

where M/M_y = non-dimensional initial yield moment
σ_w = warping stress
σ_b = bending stress

McManus (1971) used mathematical modeling and curve fitting to develop the buckling strength equation for a horizontally curved girder. The equation takes the following form:

$$F_{bc} = F_{bs}\rho_b\rho_w \qquad [2.6]$$

where F_{bs} is the buckling capacity of the compression flange modified for the effect of horizontal curvature, ρ_b, and the stress gradient caused by warping, ρ_w. The buckling capacity of the compression flange is given as:

$$F_{bs}=0.55\left[1-3\left(\frac{L}{b}\right)^2\frac{F_y}{\pi^2 E}\right] \quad [2.7]$$

$$\rho_b=\frac{1}{1+(L/R)(L/b)\left[1-\frac{L/b}{500}\right]} \quad [2.8]$$

$$\rho_w=\frac{1}{1+(F_w/F_{bc})\left[1-\frac{L/b}{75}\right]} \quad [2.9]$$

$$\rho_w=\frac{0.95+(L/b)/\left[30+8000(0.1-L/R)^2\right]}{1-0.6(F_w/F_{bc})} \quad [2.10]$$

where
F_{bc} = allowable bending stress in curved beam
F_{bs} = allowable bending stress in straight beam
ρ_b = bending stress
ρ_w = lateral flange bending or warping stress
F_y = yield strength
E = modulus of elasticity
L = unsupported length of compression flange
R = radius of curvature
b = total flange width
F_w = normal stress due to lateral flange bending or warping

The two equations for ρ_w were necessary because of the different behaviour associated with a positive or negative flange moment at the brace points. For the case where the applied flange moment at the lateral supports cause compression on the inner flange tip, the first equation should be used. For the case where the lateral flange bending produces compression at the lateral supports on the outer flange tip, both equations must be checked, and the smallest value of F_{bc} is used (McManus 1971).

2.6 Design Standards

2.6.1 AASHTO

When determining the flexural resistance of composite girders in negative flexure or non-composite sections in negative and positive flexure, the current AASHTO *LRFD Bridge Design Specifications, 6th Edition* uses the one-third rule described previously

(AASHTO 2012). The lateral bending stress is only considered for discretely braced flanges. The nominal flexural resistance of the flange, F_{nc}, depends on whether the flange is in tension or compression. Discretely braced flanges in compression shall meet the requirements described by Equation 2.11 for the strength limit state.

$$f_{bu} + A\frac{1}{3}f_l \leq \phi_f F_{nc} \qquad [2.11]$$

where f_{bu} = flange stress calculated without consideration of flange lateral bending
f_l = flange lateral bending stress
A = amplification factor when the flexural stresses are determined from first-order analysis
= $\left(\frac{0.85}{1-f_{bu}/F_{cr}}\right)$
ϕ_f = resistance factor for flexure
F_{nc} = nominal flexural resistance of the flange
F_{cr} = elastic lateral torsional buckling stress

The nominal flexural resistance, F_{nc}, used in Equation 2.11 is calculated using Equations 2.12 to 2.16. Equation 2.12 is for compression flanges that are of Class 1 or 2, *i.e.*, they can yield over the entire width before local buckling. For Class 3 or 4 flanges the flange resistance is calculated using Equation 2.13. Equations 2.14, 2.15, and 2.16 are used to calculate F_{nc} based on the lateral torsional buckling resistance of the member between points of lateral support. If the member can achieve the full-capacity of the section, Equation 2.14 will govern. If the member will fail by inelastic lateral torsional buckling, Equation 2.15 will govern. If the member fails by elastic lateral torsional buckling, Equation 2.16 will govern. The lowest nominal flexural resistance will govern, and it is either based on the cross-section strength (Equations 2.12 and 2.13) or the member stability (Equations 2.14, 2.15, and 2.16). F_{nc} is calculated in the same manner for straight and horizontally curved girders.

If $\lambda_f \leq \lambda_{pf}$, then:

$$F_{nc} = R_b R_h F_{yc} \qquad [2.12]$$

Otherwise:

$$F_{nc} = \left[1 - \left(1 - \frac{F_{yr}}{R_h F_{yc}}\right)\left(\frac{\lambda_f - \lambda_{pf}}{\lambda_{rf} - \lambda_{pf}}\right)\right] R_b R_h F_{yc} \qquad [2.13]$$

where λ_f = slenderness ratio for the compression flange

$$= \frac{b_{fc}}{2t_{fc}}$$

λ_{pf} = limiting slenderness ratio for a compact flange

$$= 0.38\sqrt{\frac{E}{F_{yc}}}$$

λ_{rf} = limiting slenderness ratio for a non-compact flange

$$= 0.56\sqrt{\frac{E}{F_{yr}}}$$

R_b = web load-shedding factor

R_h = hybrid factor

F_{yc} = specified minimum yield strength of compression flange

b_{fc} = full width of the compression flange

t_{fc} = thickness of the compression flange

F_{yr} = nominal yield stress including residual stress effects

E = modulus of elasticity, 200 000 MPa for steel

The lateral torsional buckling resistance of prismatic members is calculated by the following equations:

If $L_b \leq L_p$, then:

$$F_{nc} = R_b R_h F_{yc} \qquad [2.14]$$

If $L_p < L_b \leq L_r$, then:

$$F_{nc} = C_b \left[1 - \left(1 - \frac{F_{yr}}{R_h F_{yc}}\right)\left(\frac{L_b - L_p}{L_r - L_p}\right)\right] R_b R_h F_{yc} \leq R_b R_h F_{yc} \qquad [2.15]$$

If $L_b > L_r$, then:

$$F_{nc} = F_{cr} \leq R_b R_h F_{yc} \quad [2.16]$$

where L_b = unbraced length

L_p = limiting unbraced length to achieve nominal flexural resistance of $R_b R_h F_{yc}$ under uniform bending

$$= 1.0 r_t \sqrt{\frac{E}{F_{yc}}}$$

L_r = limiting unbraced length to achieve onset of nominal yielding in either flange under uniform bending with consideration of compression-flange residual stress effects

$$= \pi r_t \sqrt{\frac{E}{F_{yr}}}$$

C_b = moment gradient modifier

F_{cr} = elastic lateral torsional buckling stress

r_t = effective radius of gyration for lateral torsional buckling

2.6.2 CAN/CSA S6-06

The design provisions for horizontally curved steel I-girders in the Canadian Highway Bridge Design Code (CHBDC) are based on the 1993 Guide Specifications (AASHTO 1993). Both compression and tension flanges must meet the cross-section strength interaction equation:

$$\frac{M_{fx}}{M_{rx}} + \frac{M_{fw}}{M_{ry}} < 1 \quad [2.17]$$

where M_{fx} = factored bending moment due to flexure about the strong axis

M_{rx} = $\phi_s F_y S_x$

M_{fw} = factored bending moment in the flange due to torsional warping

M_{ry} = $\phi_s F_y S_y$

S_x = elastic section modulus of the girder about its major axis

S_y = elastic section modulus of the flanges only about the girder web

In addition to Equation 2.17, the compression flange must meet the stability requirements as detailed in Equations 2.18 and 2.19.

$$M_{fx} \leq M'_{rx} \quad [2.18]$$

$$M'_{rx} = \phi_s F_y S_x \left(1 - 3\lambda^2\right) \rho_b \rho_w \quad [2.19]$$

where ϕ_s = resistance factor for steel

F_y = specified minimum yield stress

λ = slenderness of the laterally unsupported segment

$$= \frac{L}{2b}\sqrt{\frac{F_y}{\pi^2 E}}$$

ρ_b = horizontal curvature correction factor

$$= \frac{1}{1 + \left[\frac{L}{R}\right]\left[\frac{L}{2b}\right]}$$

ρ_w = warping stress correction factor, taken as the smaller of ρ_{w1} and ρ_{w2} when f_w/f_b is positive

= ρ_{w1} when f_w/f_b is negative

where ρ_{w1} = $$\frac{1}{1 - \frac{f_w}{f_b}\left[1 - \frac{L}{150b}\right]}$$

ρ_{w2} = $$\frac{0.95 + (L/2b)/\left[30 + 8000(0.1 - L/R)^2\right]}{1 + 0.6\left(f_w/f_b\right)}$$

f_b = flexural stress due to the larger of the two moments at either end of the braced segment

f_w = co-existing warping normal stress

The correction factors and slenderness parameter are calculated using the unbraced length, radius of curvature, flange width, as well as the warping stress to flexural stress ratio. The f_w/f_b value is positive when f_w is compressive on the inner curved flange tip.

As discussed previously, the design equations in S6-06 were based on AASHTO's 1993 Guide Specifications, which were based research conducted up to the 1970s. At that time, second-order analyses were not commonly used for design. Therefore, there are no provisions for amplifying first-order analysis results or neglecting amplification if a second-order analysis was done. The equation was designed assuming a first-order analysis was used.

2.6.3 CAN/CSA S6-14

The CHBDC has adopted new design provisions for horizontally curved girders (CSA 2014). The equation takes the form shown in Equation 2.20 (CSA 2014):

$$\frac{M_{fx}}{M_{rx}} + U_c \frac{w_c M_{fw}}{M_{ry}} \leq 1 \qquad [2.20]$$

where M_{fx} = factored moment about the strong axis of the girder
M_{rx} = moment resistance about the strong axis, for braced or unbraced condition as the case may be
M_{fw} = factored bending moment in the flange due to warping
M_{ry} = moment resistance of section about the weak axis
w_c = 0.5 when the lateral bending moment in the flange has major reversals, equal to 1.0 otherwise
U_c = amplification factor when the factored moments are determined using first-order analysis
$= \left(\frac{0.85}{1 - M_{fx}/M_u} \right)$

where M_u = the elastic lateral torsional buckling moment resistance for a straight girder segment

2.7 Further Research Needs

In Canada, Class 4 flanges are not typically used in new bridges, although existing bridges can sometime fail to meet the Class 3 flange requirement. After review of the available test results and FEA data from girders with Class 3 flanges or better, it was found that all of the specimens reached at least 81% of their yield moment. This indicates that all the available data covers only inelastic lateral torsional buckling. In addition, the majority of the applicable data comes from White *et al.* (2001) which investigated mostly Class 4 flanges and very limited number of Class 3 or better sections. Only two different compression flange slenderness were investigated that met at least the requirements of a Class 3 section. To update the design equations for horizontally curved girders in CSA-S6-06 with confidence, more information is required for LTB failure in the elastic range and for girders with a wider range of flange slenderness.

CHAPTER 3

FINITE ELEMENT MODELING

3.1 Overview

ABAQUS Version 6.12 finite element analysis software (Dassault 2012) was used to develop the numerical models for the parametric study. Horizontally curved plate girders were modeled with a range of flange and web plate sizes, stiffener requirements, and radii of curvature. Radial bracing, boundary support conditions, and loading configurations that are representative of highway steel bridge girders were incorporated. The finite element (FE) models were validated with previous experimental testing and numerical analysis.

3.2 FEA Discretization

The general-purpose four-node reduced integration shell element S4R was used to model horizontally curved plate girders. This element uses thick-shell theory as the shell thickness increases, and becomes a discrete Kirchoff thin-shell element as the thickness decreases (Dassault 2012). Shell elements are used to model structures in which one dimension, the thickness, is significantly smaller than the other dimensions (Dassault 2012). Schumacher *et al.* (1997) and Grondin *et al.* (1998) demonstrated that shell S4R elements are appropriate for modeling steel plate structures. The two-node beam, B31, element was used for modeling the bracing and stiffeners. It is applicable for modeling thick as well as slender beams and allows for transverse shear deformation (Dassault 2012). Both B31 and S4R have all six degrees of freedom active at each of their nodes.

3.2.1 Girders

The web contained 20 elements along its depth, while the flanges used 10 elements across its width. Using this mesh refinement in the flange and web created desirable shell aspect ratios between 1.0 and 2.9 for the 100 mm tangential element length. Because the normal stress in an element is taken at the centre of the element, the normal stress at the flange

tip was obtained by extrapolation. The single girder was partitioned into three segments to ensure the radially fixed nodes were at the locations of the cross-frames, since the cross-frames were not incorporated in the model. The approximate 100 mm element length was obtained by adjusting the number of longitudinal elements in each partition. Using a constant element length of 100 mm meant that the aspect ratio for all shell elements in the webs and flanges was less than 3:1. However, for the flange elements in the parametric models with the 175 mm wide flanges, the aspect ratio was 5.7:1. All models had shell aspect ratios less than 10, which is the recommended maximum for quadrilateral elements in ABAQUS (Dassault 2012). The numerical models for the few girders that had a slightly higher aspect ratio for only the flange elements appeared to perform similarly to the other models. Thus, the higher than ideal aspect ratio was determined to not be of concern. Figure 3-1 shows the shell element meshing.

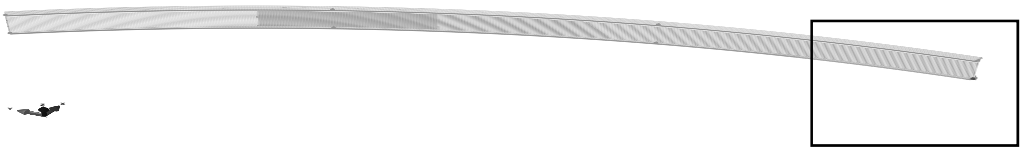

(a)

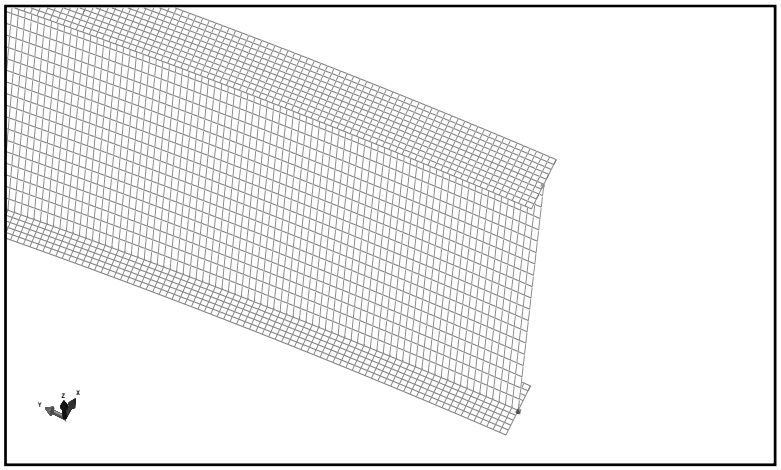

(b)

Figure 3-1: Shell element meshing (a) full-length (b) girder end

3.2.2 Stiffeners

B31 beam elements were used to model the stiffeners. Full-depth stiffeners welded to the web and flanges were located at vertical supports, as well as cross-frame locations where the vertical point loads were applied. Partial-depth intermediate stiffeners welded to the top flange and web were included if they were required as stated in the provisions for straight plate girders in CSA S6-06. The stiffener elements shared the same nodes as the shell elements. The vertical stiffener elements located along the web were defined such that the stiffener width was equal to the flange width (stiffeners extended from the web to the flange tips, on each side). Because these stiffener elements were only attached to the web nodes, they would not prevent relative rotation between the web and the flange. In order to restrain this rotation, stiffener elements were also placed across the flange width. These elements were defined to have a height equal to half the depth of the girder web. The loading condition did not include the self-weight of the member, so this "extra" stiffener material would not increase the load on the member. Figure 3-2 shows the stiffener elements.

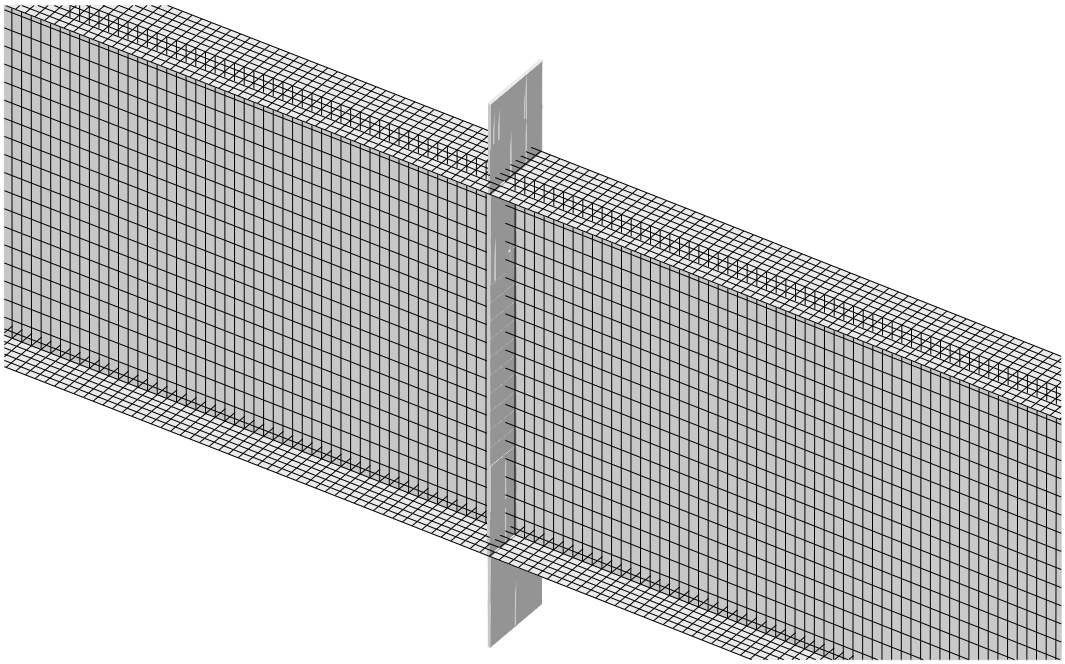

Figure 3-2: Full-depth stiffeners

3.3 Material Properties

A stress-strain curve for ASTM A572 Grade 50 steel (F_y = 345 MPa) was used for the parametric study conducted by White *et al.* (2001). All girder and stiffener elements in the parametric study presented in Chapter 4 used CSA G40.21-13, Grade 350W steel (F_y = 350 MPa). An engineering stress-strain curve similar to that used by White *et al*. (2001) was used for this work. The modulus of elasticity was taken as 200 000 MPa and the yield strength as 350 MPa. A yield plateau was defined with a modulus of zero. Onset of strain-hardening takes place at a strain of 0.02112 and the strain-hardening range was defined by four points as shown in Figure 3-3.

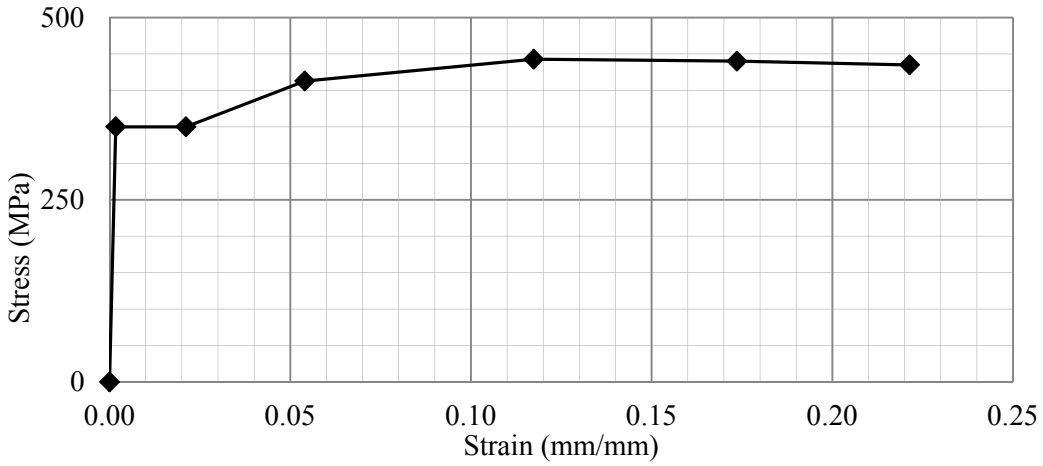

Figure 3-3: Typical engineering stress-strain curve for 350W steel

An isotropic material model, defined by the modulus of elasticity of 200 000 MPa and Poisson's ratio of 0.3, was used. Yielding of the material starts at 350 MPa. The FE model requires true stress, σ_{true}, and true strain, ε_{true}, properties, and the true strain is defined using the plastic strain only, which is the total strain minus the elastic strain. The true stress and strain were calculated using Equations 3.1 and 3.2.

$$\varepsilon_{true} = ln(1+\varepsilon_{eng}) \quad [3.1]$$

$$\sigma_{true} = \sigma_{eng}(1+\varepsilon_{eng}) \quad [3.2]$$

where σ_{true} = engineering stress
ε_{true} = engineering strain

Table 3-1 shows the conversion from engineering to true stress and strain. The true strain can be separated into an elastic component and a plastic component. Columns 3 and 5

show the input values of true stress and plastic strain used to define the inelastic portion of the material response.

Table 3-1: Stress-strain response for 350W steel

Engineering		True		
Stress	Strain	Stress	Total Strain	Plastic Strain
σ_{eng} (MPa) (1)	ε_{eng} (mm/mm) (2)	σ_{true} (MPa) (3)	ε_{true} (mm/mm) (4)	(mm/mm) (5)
350.0	0.001722	350.6	0.001721	0
350.0	0.021120	357.4	0.020900	0.01911
412.8	0.054000	435.1	0.052590	0.05041
442.8	0.117400	494.8	0.111000	0.10850
440.1	0.173600	516.5	0.160100	0.15750
440.9	0.221400	531.3	0.200000	0.19730

3.4 Loading Conditions

All girders used for the parametric study were subjected to a uniform bending moment in the middle third of the span. This was achieved by applying point loads to the top web-to-flange junction, at the intermediate cross-frame locations. This four-point bending configuration created a constant bending moment in the centre segment, which was the segment under consideration. As stated previously, full-depth stiffeners were used at the load points and at the supports to prevent web distortion at those locations. The girder self-weight was not included in the analysis.

It should be noted that the end segments provide lateral torsional buckling restraint to the centre segment because of the more favourable bending moment in these segments. To eliminate the restraint provided by the end spans several attempts were made to create a parametric study with only the middle segment. A straight girder was modeled and checked against the theoretical buckling capacity. The variations of single span configurations included the following:

- Concentrated end rotations applied to the centroid of the girder with constraint equations to force the girder end to remain plane during the loading process;
- Concentrated end rotations applied to the centroid of the girder with “rigid” elements at the girder ends to force the girder ends to remain plane.

- Applying longitudinal force couples at the girder ends only at the web-flange junction nodes;
- Applying longitudinal force couples at the girder ends only along the flange nodes;
- Applying longitudinal force couples at the girder ends along all nodes and proportional to the linear stress distribution.

Unfortunately, none of these methods of creating a constant moment in girder segment produced analysis results that matched the theoretical values, probably due to boundary condition issues. However, the three-segment girder, with the end segments lengthened to buckle at the same time as the centre span, did match the theoretical value. The length of the end segments were calculated by equating the critical buckling moments in each span. The critical buckling moment for the centre span was calculated using a moment gradient factor ($\omega_2 = 1.0$) because it is under uniform bending moment. The critical buckling moment for the end segments was calculated using a moment gradient factor ($\omega_2 = 1.75$) because of the moment gradient. The length of the end span was varied until its critical buckling moment matched that of the centre span. Sample calculations of this work are presented in Appendix A.

3.5 Boundary Conditions

A cylindrical coordinate system was used to define boundary conditions, apply loads, and obtain analysis results. Vertical supports were located at the girder ends. The vertical restraints were only applied to the bottom web-flange junction node. This allowed the ends to rotate freely in the tangential plane. A tangential restraint was applied at the bottom web-flange junction node, at one end only. This meant the girder was simply-supported in the tangential direction. Radial restraints were provided at the top and bottom web-to-flange junction nodes, at the two load points and the two supports. Figure 3-4 shows the boundary conditions. As stated previously, stiffeners were provided at the load points and at the vertical support locations.

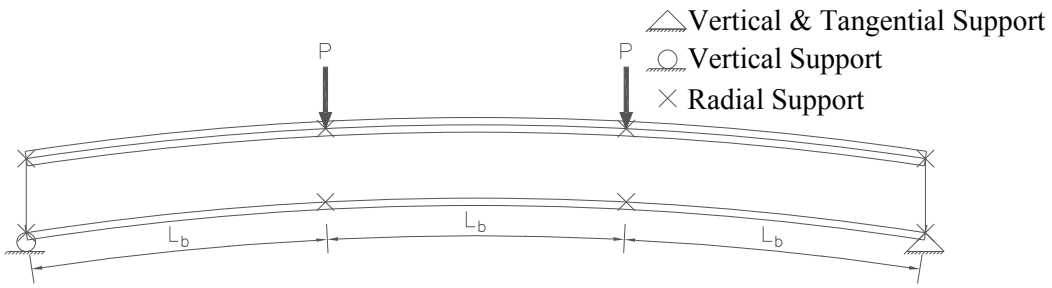

Figure 3-4: Boundary conditions

3.6 Residual Stresses

Longitudinal residual stresses were included as initial stresses prior to applying the point loads. The residual stresses used for the girders were based on flange and web plates that were flame-cut and then welded together. This fabrication procedure creates tensile residual stresses equal to the yield strength of the plate at the flange tips and at the web-to-flange junctions. The remaining regions have compressive residual stresses that equilibrate the large tensile stresses. Figure 3-5 shows a simplified residual stress pattern modeling this fabrication procedure.

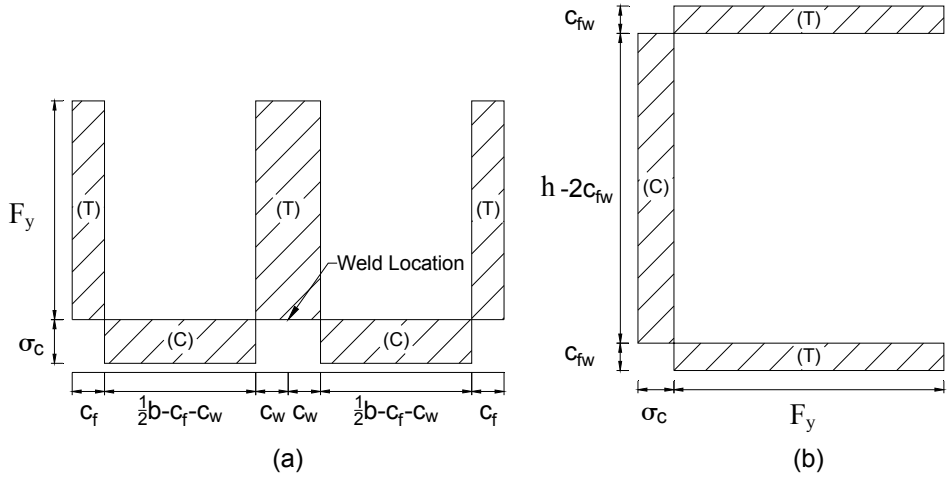

Figure 3-5: Simplified residual stress distribution in flame-cut and welded (a) flange plate (b) web plate (ECCS 1976)

Referring to Figure 3-5, the residual stresses were calculated using the procedure outlined in ECCS (1976). For plates flame-cut along both edges, the tensile residual stresses, F_y, at the tips are equal to the yield strength of the plate, and the width, c_f, of the tension block shown in Figure 3-5a is calculated using Equation 3.3. For welded plates, the width of the

tension block, c_w, adjacent to the weld is calculated using Equation 3.4. This equation is only applicable for continuous, single pass welds, which is typical in bridge girder fabrication. For web plates that had their edges flame-cut prior to welding, Equation 3.5 is used to calculate the tension block width, c_{fw}. The effect of welding an edge that was previously flame-cut does not result in the algebraic addition of tension block widths, since the weld heat tends to relieve the tensile residual stress due to flame-cutting (ECCS 1976). After the widths of all stress blocks are calculated, the magnitude of compressive residual stress, σ_c, in each plate is calculated by equilibrating the total compressive force with the total tensile force in each plate.

$$c_f = \frac{1100\sqrt{t}}{F_y} \quad [3.3]$$

$$c_w = \frac{12000 p A_w}{F_y \Sigma t} \quad [3.4]$$

$$c_{fw}^4 = c_f^4 + c_w^4 \quad [3.5]$$

where
c_f = tension block width due to flame-cutting alone
t = plate thickness
F_y = plate yield strength
c_w = tension block width due to welding alone
p = process efficiency factor, 0.90 for submerged arc welding
A_w = cross-sectional area of added weld metal
Σt = sum of the plate thickness meeting at the weld
c_{fw} = final tension block width, including flame-cutting and welding

After the residual stresses were calculated as described above using the ECCS (1976) method, they needed to be adjusted so they could be applied to the elements in the model, which were not the same width as the calculated stress blocks. The stresses were adjusted to suit the element width. For example, the initial stresses applied to the elements along the flange tip were calculated by determining the resultant longitudinal stress that is present within the width of the element. Figure 3-6 shows an example of what the difference between calculated residual and initial input stresses could be for a flange plate. The values shown in Figure 3-6 are not for a specific plate, but are used to give a sense of the magnitude of the difference. Full sample calculations of the residual stresses as well as the initial stresses input to the model information are included in Appendix A.

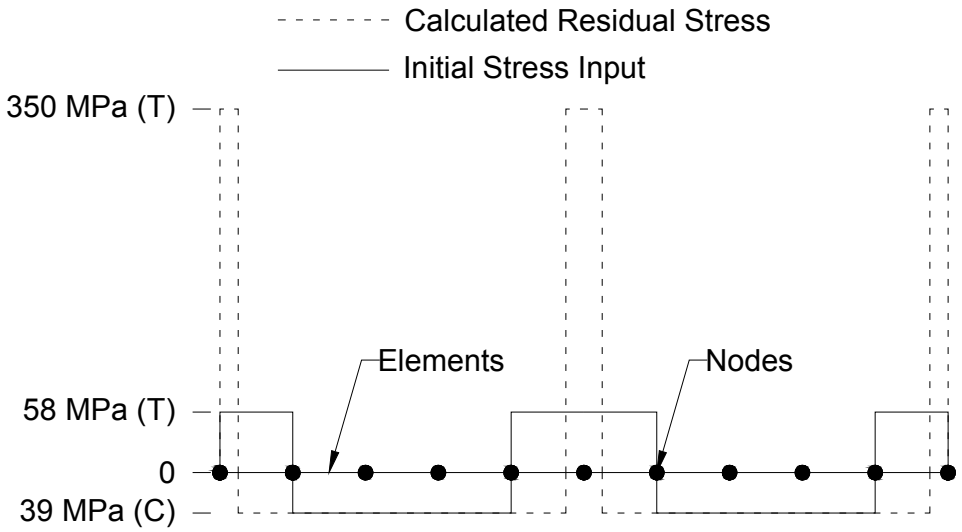

Figure 3-6: Theoretical example flange plate residual stress profile

After the initial stresses were input to the model, an "Equilibrium" load step was created to verify the calculations. The Equilibrium step occurred before any external loads were applied, and after the initial stresses were defined. At the conclusion of the step, the longitudinal stresses were checked to confirm they were close to the initial input stresses.

3.7 Nonlinear Analysis

A nonlinear analysis, including large displacements and large strains was conducted using the Riks solution strategy implemented in ABAQUS. The Riks method uses the "arc length" along the static equilibrium path in load displacement space, which allows solutions regardless of whether the response is stable or unstable (Dassault 2012). Curved girders experience larger horizontal displacements due to the lateral moment and torsion that are created. For this reason, nonlinear geometry was included in the analysis. Using the nonlinear geometric analysis allowed for the second-order bending effects to be accounted for.

The Riks algorithm in ABAQUS automatically adjusts the load increment size as the analysis progresses to optimize computation time. In order to determine the moment capacities based on the various design equations the load needed to be incremented in small amounts. This was done by initially determining the ultimate capacity with no restrictions on the increment size. Once that was determined, the increment size was fixed to be 1% of the total load. This allowed for analysis output for every 1% increase in the

load. This meant there were 100 load increments from which output data could be obtained for each model.

3.8 Validation of Finite Element Model

In order to conduct a parametric study, the FEA model needed to be validated by other experimental tests and numerical analyses. FEA models were developed and compared with three experiments conducted by Hartmann (2005) and one FEA conducted by White *et al.* (2001). The results of the comparison are shown in Table 3-2. The validation procedure is described in Sections 3.8.2 and 3.8.3.

Table 3-2: Finite element model validation

Specimen Identification	Moment Capacity		Moment Capacity	Variance
	M_{r1} (other source) (kN·m)	$\left(\frac{M_r}{M_y}\right)_1$	M_{r2} (this study) (kN·m)	
Hartmann-B1	4539	0.92	4417	-2.7%
Hartmann-B5	5278	0.92	5081	-3.7%
Hartmann-B6	6400	0.94	6086	-4.9%
White-2.75-15-160-3-0.050-0.50	4887	0.82	5168	+5.4%

The FE model presented in this chapter compares well with previous test and analysis results having less than 5% difference with the test results and 5.4% higher capacity predicted by the model of White *et al.* (2001). This close agreement provides confidence that the FE model can be used to expand the database of lateral torsional buckling failure data for horizontally curved steel I-girders.

3.8.1 Curved Bridge Model (CISC 2010)

The first step in the validation process of an FE model was to compare the analysis results from the model with those of a linear elastic analysis model of a horizontally curved bridge. Such a comparison involves fewer uncertainties than either a large scale test specimen or an advanced finite element model presented by Hartmann (2005) and White *et al.* (2001). For this part of the validation process, bridge design example 3 of the CISC (2010) steel bridge design course was selected. The CISC design example of a horizontally curved bridge consists of a three-span, continuous, composite steel-concrete bridge with four parallel I-girders. The radius of curvature is 200 m at the bridge

centerline. The span lengths are 49.0 m, 63.7 m, and 49.0 m, for a total length of 161.7 m along the centreline. Cross-frames between girders are spaced at 4.9 m on average, for a total of 34 cross-frames along each girder line. Horizontal bracing is provided at the bottom flange level in the outer bay, throughout the entire length of the bridge. The bridge layout for the CISC design example is shown in Figure 3-7. The support locations are labelled with the associated cross-frame (CF) number.

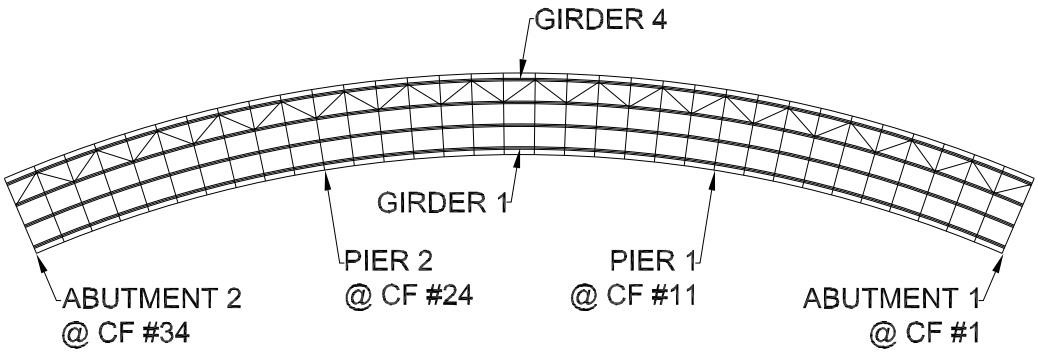

Figure 3-7: Plan view of the CISC design example

3.8.1.1 CISC Model

The sample bridge, used as a design example, was modelled using a combination of 3-D beam elements and shell elements (CISC 2010). The software used was a non-commercial software developed by a CISC employee. The concrete slab and steel web were modeled using shell elements. Uncracked concrete properties were used for the slab elements. The steel flanges were modeled using beam elements. Horizontal bracing and cross-frame members were modeled using truss elements.

During placement of the concrete deck, each stage of construction required a different model. Concrete cast in previous stages was assumed to have gained sufficient strength to make the steel girders and concrete slab act fully composite during the following deck casting stage. To account for concrete creep, the steel-concrete modular ratio was taken as 3n, *i.e.*, the modulus of elasticity of the concrete was taken as one-third of the short term modulus of elasticity. At the segments where the concrete slab had not been placed and at the segment where the concrete is just being placed, only the bare steel section was modeled. The superelevation of the roadway and girders was not considered in the model geometry.

The girder web was modeled using a single rectangular shell element over the full depth, and two shell elements were used between cross-frames (CISC 2010). The stresses and forces were computed at cross-frame locations and mid-way between cross-frames. The longitudinal subdivision was selected to model lateral bending of the top flange with sufficient accuracy. When modeling composite sections, the centre of gravity of the concrete slab was assumed to lie in the same plane as the centre of gravity of the top flange for simplicity. The concrete barriers were not included in the model.

With four girders, two piers and two abutments, there are 16 bearing locations of support boundary conditions. Tangential displacements were prevented at only one pier while radial displacements were prevented at the inner bearing of each pier and abutment. Vertical displacements were prevented at all 16 bearing locations. The bearings were located at the intersection of the bottom flange and the web.

3.8.1.2 ABAQUS Model

Six models were created in ABAQUS to compare with the CISC design example. Six models were required to determine the vertical deflections throughout the construction staging. The principle of superposition was applied to determine the deflections at the appropriate concrete casting stage. Both the CISC design example and models created in ABAQUS used unfactored loads. The six models created were based on the construction stages depending on the loading conditions and composite regions described as follows:

Stage 1: Steel self-weight only
Stage 2: Formwork and rebar over entire length
Stage 3: Wet concrete between cross-frames 1 and 6 (see Figure 3-7)
Stage 4: Composite between cross-frames 1 and 6, with wet concrete between cross-frames 15 and 20
Stage 5: Composite between cross-frames 1 and 6 and between cross-frames 15 and 20, wet concrete between 24 and 34
Stage 6: Composite between cross-frames 1 and 6, 15 and 20 and 24 and 34, with wet concrete between 6 and 11

General views of the FE models during Stage 1 and Stage 6 are shown in Figure 3-8 and Figure 3-9, respectively.

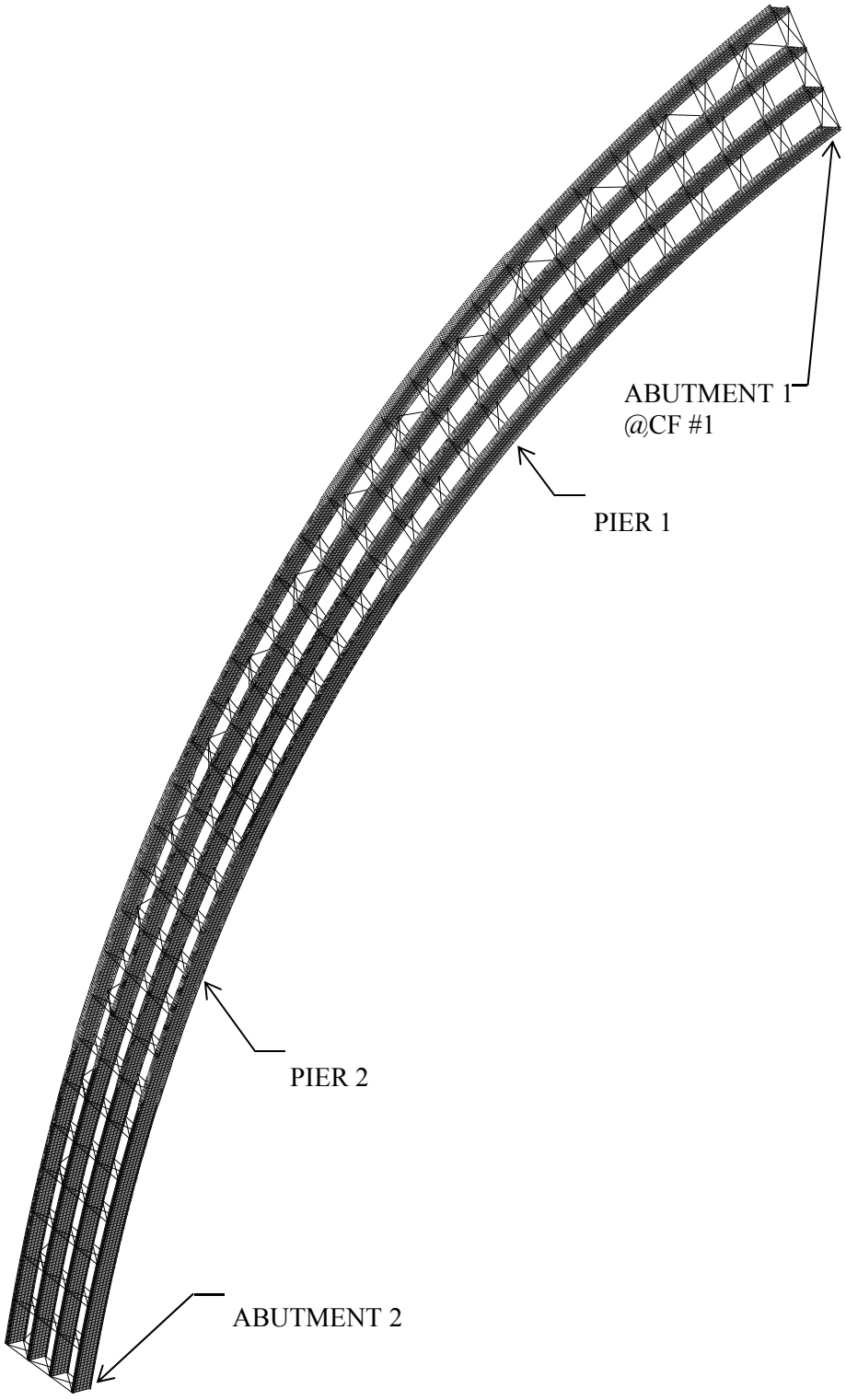

Figure 3-8: ABAQUS model for construction Stage 1

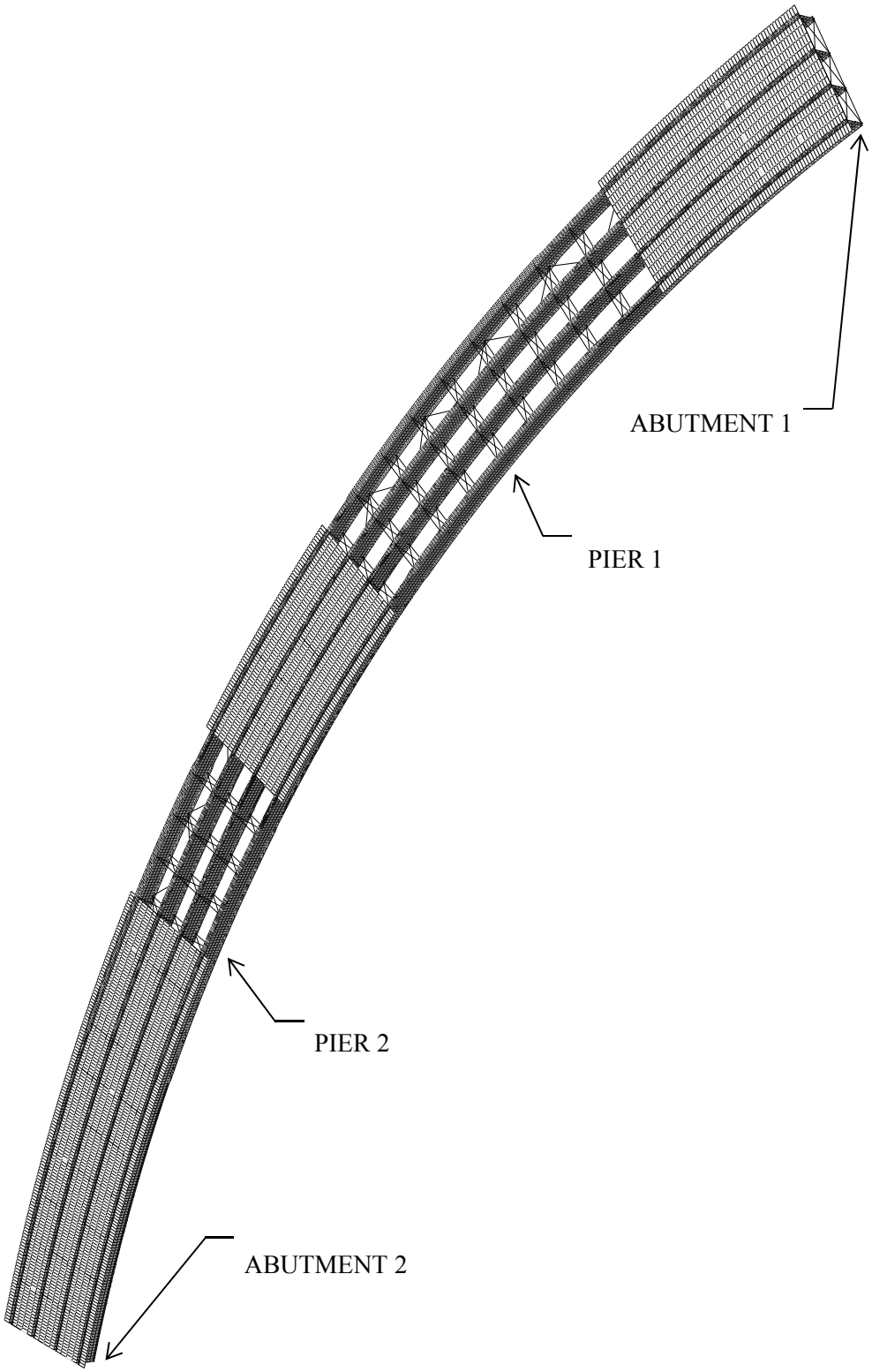

Figure 3-9: ABAQUS model for construction Stage 6

The steel girder web and flanges were modeled using S4R shell elements. The flanges were modeled using four elements across the width and the web was modeled with five elements through the depth of the section. Longitudinally, the web and flanges were modeled with 15 elements between cross-frames to keep the aspect ratio of the rectangular shell element to a value less than 3.0. The girder geometry was partitioned to allow for the elements to have varying thicknesses and flange widths to suit the girder sections and cross-frame layout used in the CISC design example. The shell element thickness was centered on the nodes, thus the centroids of the top and bottom flanges were located at the top and bottom of the girder web, respectively. At field and shop splice locations where the flange width changed, the nodes across the interface of flanges were merged to create an "average" flange width at the splice location. The varying thicknesses at shop and splice locations did not require any "averaging" techniques; the actual flange thicknesses were used on both sides of the splice.

The cross-frames were modeled using the 3-D linear displacement truss element T3D2. The horizontal and diagonal cross-frame elements and horizontal bracing elements were all connected to the girders at the flange-to-web junction, sharing a node with the girder flange, the web and the diaphragm stiffener. The truss elements of the cross-frames and horizontal bracing and shell elements of the girder webs and flanges would all share the same node, if all members connected to the same point.

The composite concrete deck was modeled using the same type of shell element as for the steel girders, the S4R element. Radially, four elements were used between girder lines and one element for the slab overhangs. Longitudinally, 15 elements were used between cross-frames and the deck slab was partitioned to align the slab nodes with the girder nodes. The slab was connected to the girder flange-web junctions by sharing the same nodes. The centroid of the slab elements was therefore located at the same elevation as the centroid of the top flange, which is consistent with the CISC model. The shell thickness for all concrete slab elements was 235 mm.

The CISC design example used only one shell element throughout the depth of the web. The modeled girders contained five shell elements throughout the depth of the web. This meant the modeled girder sections might result in more flexible beams than the design example. However, since the analysis is a first-order linear elastic analysis and the strain

distribution in the cross-sections is expected to be linear, the difference between the CISC model and the ABAQUS model was expected to be minimal.

Stiffeners were added to the model at the cross-frame locations. The stiffeners were modeled using B31 beam elements between the web nodes. The element's cross-section is rectangular and 400 mm by 20 mm oriented to be perpendicular to the girder web. Since the element is centered with the web, the width of the beam element is twice the width of the stiffeners. Five elements were used over the depth of the web and shared the same nodes as the web elements.

Linear elastic material properties were used for both steel and concrete elements. Cross-frames, horizontal bracing, girder webs and flanges, and stiffeners all used the same steel material model. The density of steel was set to 7850 kg/m^3 and Young's modulus was 200 000 MPa, the yield strength was taken as 350 MPa and Poisson's ratio is 0.3. The modulus of elasticity for the deck concrete was taken as 8260 MPa to suit the 3n steel-concrete modular ratio used to account for creep of the concrete. Poisson's ratio for concrete was selected to be 0.2. Because the concrete dead load was applied using point loads, the concrete material model did not include its density. However, the calculation of the applied point loads was based on a concrete density of 2400 kg/m^3, the density of normal density reinforced concrete.

Displacement boundary conditions were applied to all 16 support locations. The bottom web-flange nodes at the supports were transformed to cylindrical coordinates to correctly apply the boundary conditions. The bridge was radially restrained along Girder 1 at the bearing locations. Tangential restraint was applied to all girders at a single pier location. All girders were vertically restrained at all bearing locations.

The applied loads depended on the stage of construction under consideration. A gravity type distributed load was applied to the entire model for all construction stages. The gravitational acceleration of 9.81 m/s^2 was used to transform mass of the steel into gravity loads. The weight of the formwork and reinforcing steel was simulated using concentrated forces applied at the applicable nodes based on the tributary area for each node. The CISC design example provided uniformly distributed loads (UDL) along the girder lines, which were then converted into an equivalent point load at the nodes. From the CISC design example the weight of the concrete on the exterior and interior girders

was 18.0 kN/m and 20.9 kN/m, respectively. These resulted into 5.877 kN and 6.827 kN per node for the exterior and interior girders, respectively. The weight of the reinforcing steel corresponds to 0.49 kN/m and 0.62 kN/m for the exterior and interior girders, respectively, which results into nodal forces of 0.160 kN and 0.203 kN for the exterior and interior girders, respectively. The weight of the formwork was 2.04 kN/m and 2.59 kN/m for the exterior and interior girders, respectively. These result into 0.666 kN and 0.846 kN per node for the exterior and interior girders, respectively. All concentrated forces were applied at the top web-flange nodes. The weight of the wet concrete and reinforcing steel was applied to regions where wet concrete was being placed during the construction stage considered.

The analysis consisted of a first-order linear analysis.

3.8.1.3 Model Comparison

The vertical displacement comparison between the CISC and ABAQUS models for Stages 1 and 6 are shown in Figure 3-10. The displacements from the ABAQUS model correlate well with the deflection data provided from the CISC design example. For Stage 1, when only the self-weight of the girder members is applied, the maximum vertical displacements are within 4% for all spans respectively, for Girder 1, and within 6% for Girder 4, except for the middle span, where it reaches 10%. The increased difference in the middle span could be due to mesh "softening". The ABAQUS model uses a finer mesh, and this could be the reason for the larger displacements in the middle span for Stage 1. The maximum displacements in the end spans for Stage 6 are all within 6%. At Stage 6 the maximum displacements are within 17% and 11% for Girders 1 and 4 respectively. Assumptions were made regarding concrete haunch heights, as well as the cross-sectional area for the lateral bracing was not provided in the CISC example. These could be reasons for the difference. However, the overall girder response is very similar in both models.

The excellent agreement between the two models provided confidence in the modeller's ability to create the complex models required to pursue the model validation with Hartmann (2005) and White *et al.* (2001).

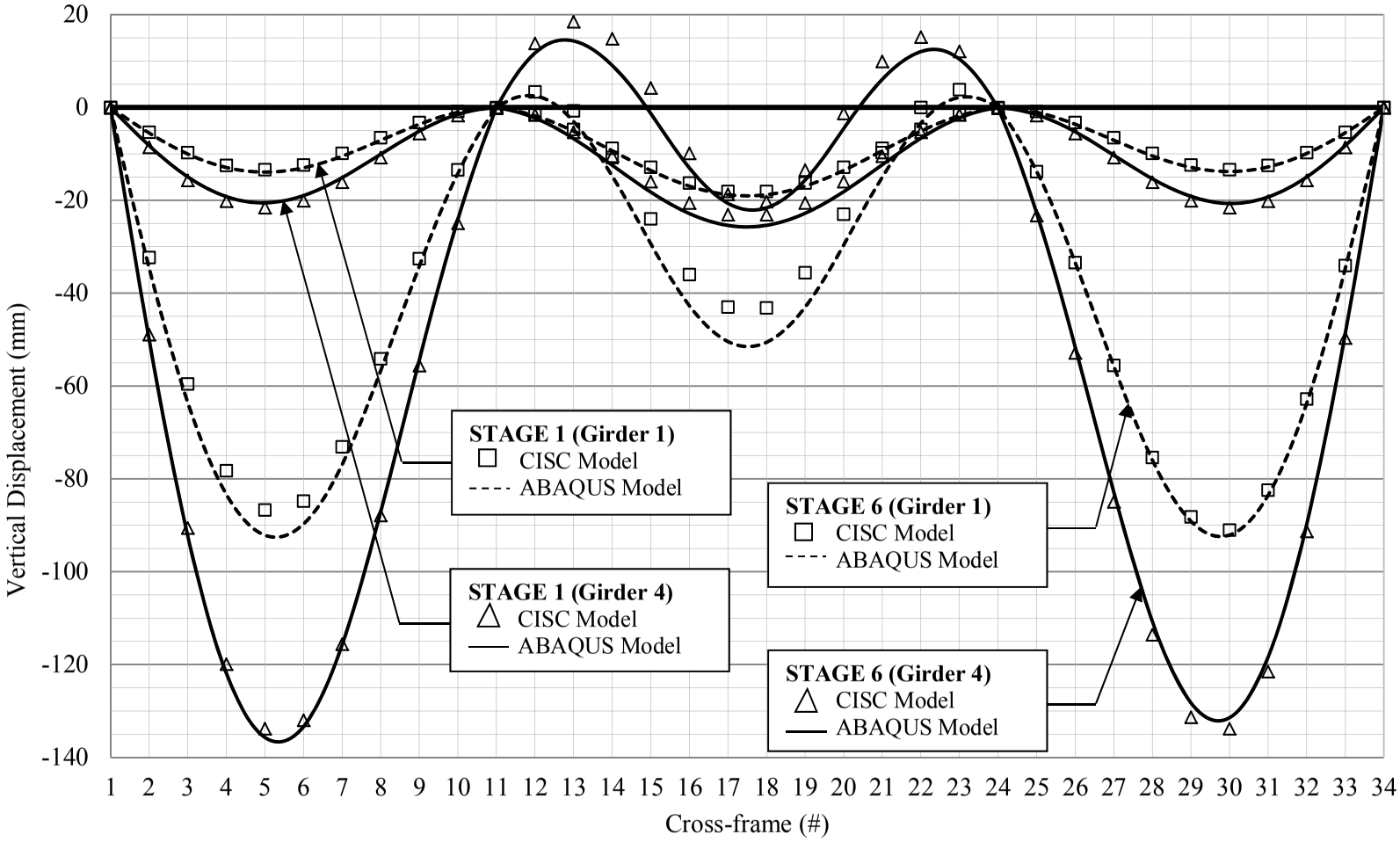

Figure 3-10: CISC and ABAQUS model comparison

3.8.2 Large Scale Girder Tests (Hartmann 2005)

The three-girder, non-composite, test frame experiment results done by Hartmann (2005) were used to validate the simple single-girder model created for the parametric study. Hartmann (2005) defined failure as the point at which a decrease in the specimen vertical bending resistance is associated with an increase in either the total load sustained by the test frame or the vertical displacement of the test frame. The entire test frame was modeled as shown in Figure 3-11. To optimize computation time, a refined mesh as described previously was used for the test specimen, and a coarse mesh was used for the remaining components of the test frame that were not being investigated. The refined mesh used for the test specimen was discretized similarly as described in Section 3.2. Beam element B31 was used to model the bracing members.

The test specimen was subjected to uniform bending moment by applying six point loads, two on each girder that were located outside the extents of the specimen. Residual stresses were incorporated as described in Hartmann (2005). Tension coupon testing was conducted on each flange and web plate for the specimens to obtain the stress-strain response. These results were used to define the material properties of each steel component. The cross-frames and horizontal bracing were modeled using beam, B31, elements as opposed to simple truss elements because the test-frame used large pipe sections with rigid connections.

Hartmann (2005) test specimens B5 and B6 were chosen to validate the FE model because the girder flanges were Class 2 and 1, respectively. All other test specimen flanges were Class 4. Test specimen B1 was also modeled because it was a doubly-symmetric girder with web slenderness, h/w, close to 150, typical for bridge girders, whereas the other doubly-symmetric specimens had stockier webs. As shown in Table 3-2, the FE results compared well with the experimental testing. The model results were within 5% of the test results.

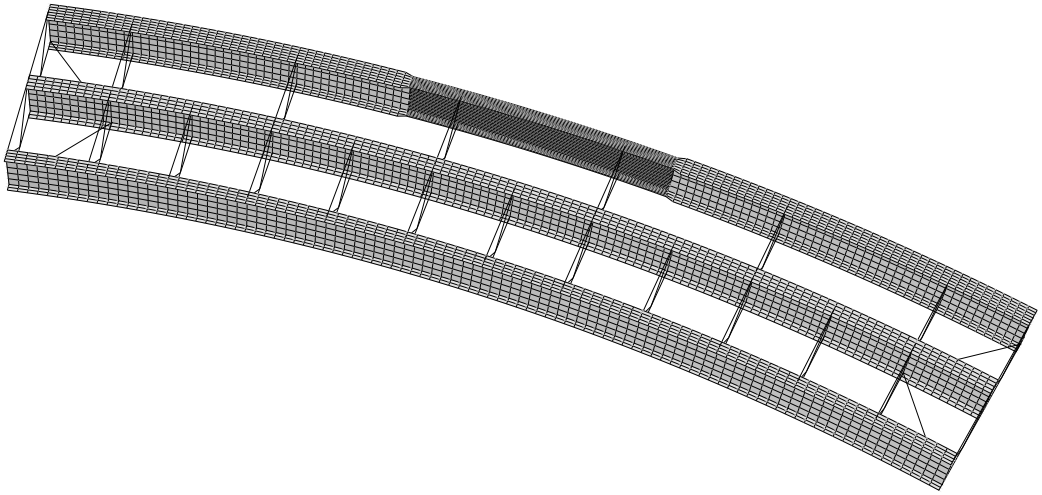

Figure 3-11: Finite element model of experimental test frame

3.8.3 Numerical Analysis (White et al. 2001)

One model from the parametric study conducted by White *et al.* (2001) was used to validate the FE model developed in this study. The parametric study by White *et al.* (2001) was used as a guideline to create a new parametric study presented in Chapter 2. White *et al.* (2001) used single girders in four-point bending to create a uniform bending moment in the middle segment. Lateral restraints were also provided at the top and bottom web-flange nodes. The elements for the entire segment were defined exactly as stated previously in this chapter.

Steel and residual stress properties were used as defined in White *et al.* (2001). Parametric analysis specimen 2.75-15-160-3-0.050-0.50 was used because it used Class 1 flanges and the web slenderness was 160, which is common for highway bridge girders. The modeled girder is shown in Figure 3-12. As shown in Table 3-2, the new model predicts a girder capacity within 6% of the capacity obtained by White *et al.* (2001).

Figure 3-12: Finite element model of previous numerical analysis

CHAPTER 4

PARAMETRIC STUDY

4.1 Overview

Various experimental tests and numerical analyses have been conducted on curved girders to determine their effect on moment capacity. Broad parameter categories that have been investigated by other researchers include loading condition, boundary conditions, cross-section dimensions, and overall member dimensions. In Canada, Class 4 flanges are not typically used in new bridges, although existing bridges can sometimes fail to meet the Class 3 flange requirement. The review of the available test and FEA data from girders with Class 3 flanges or better indicated that all of the specimens reached at least 81% of their yield moment before failing by lateral torsional buckling. In addition, the review of the literature revealed that there is only a limited range of compression flange dimensions. The lateral torsional buckling resistance of girders is generally less than 80% of the yield moment of the girder section. To update the design equations for horizontally curved girders in CSA-S6-06 with confidence, more information is required for girders where LTB failure governs and for girders with more variation in flange dimensions.

4.2 Analysis Procedure

With most structural analysis software commonly used in design offices having the capability to perform first-order and second-order analyses, designers have the option to easily conduct first or second-order analyses using elastic material properties. The effects of residual stresses and material yielding are included when they use design equations to check the capacity of the member. This meant three analyses needed to be conducted for each parametric model. One analysis that included full-nonlinear behaviour with second-order bending effects, residual stresses and inelastic material properties, provided the "actual" FEA moment resistance of the member, M_r. Two analyses that used elastic material properties without residual stresses were also performed. First and second-order analyses each provided the "calculated" moment resistance of the member, M_{calc}.

In order to determine the calculated resistance from the design equations, the load had to be incremented until the strong axis bending moment in the girder barely satisfied the design equation with the corresponding weak axis bending moment. The first and second-order elastic analysis models provided output for every 1% increase in applied load. This provided enough results to determine accurately the maximum moment for each design equation. For each equation the calculated bending resistance about the strong axis depended on the applied moments about the strong and the weak axis bending. The moments about the weak axis were obtained from the normal stresses in the flanges. The strong axis moment at the point where the design equations reach their limit corresponds to the calculated moment resistance, M_{calc}. It should be noted that this approach is not typical for design; the design process consists of checking the design equation with the weak axis and strong axis factored moments. The strong axis bending moment at each load increment was obtained from a "section-cut" in the finite element model in the centre of the span. The corresponding weak axis bending moment, or lateral bending stress used for the AASHTO equation, was derived as shown in the sample calculations in Appendix A.

4.3 Analysis Parameters

The dimensions of the girders modeled in this parametric study are presented in Table 4-1. A uniform bending moment in the middle segment was applied to all models, with the boundary conditions as described in Chapter 3. All girder plates and stiffeners were modeled with the same steel properties and hybrid girder sections were not considered. All models consisted of single girders only.

Table 4-1: Description of models in the parametric study

Model	Specimen ID*	Flange			Web			Radius	Unbraced Length
	h/w - b/2t -R	*b*	*t*	Class	*h*	*w*	Class	*R*	*L*
(#)		(mm)	(mm)		(mm)	(mm)		(m)	(mm)
1	075-4.61-100	175	19	1	1000	13.3	2	100	8000
2	075-4.61-450	175	19	1	1000	13.3	2	450	8000
3	075-4.61-750	175	19	1	1000	13.3	2	750	8000
4	075-4.61-1000	175	19	1	1000	13.3	2	1000	8000
5	075-8.33-100	350	21	2	1000	13.3	2	100	8000
6	075-8.33-450	350	21	2	1000	13.3	2	450	8000
7	075-8.33-750	350	21	2	1000	13.3	2	750	8000
8	075-8.33-1000	350	21	2	1000	13.3	2	1000	8000
9	075-10.63-100	425	20	3	1000	13.3	2	100	8000
10	075-10.63-450	425	20	3	1000	13.3	2	450	8000
11	075-10.63-750	425	20	3	1000	13.3	2	750	8000
12	075-10.63-1000	425	20	3	1000	13.3	2	1000	8000
13	100-4.62-100	425	46	1	2000	20	3	100	8000
14	100-4.62-450	425	46	1	2000	20	3	450	8000
15	100-4.62-750	425	46	1	2000	20	3	750	8000
16	100-4.62-1000	425	46	1	2000	20	3	1000	8000
17	100-8.33-100	500	30	2	2000	20	3	100	8000
18	100-8.33-450	500	30	2	2000	20	3	450	8000
19	100-8.33-750	500	30	2	2000	20	3	750	8000
20	100-8.33-1000	500	30	2	2000	20	3	1000	8000
21	100-10.34-100	600	29	3	2000	20	3	100	8000
22	100-10.34-450	600	29	3	2000	20	3	450	8000
23	100-10.34-750	600	29	3	2000	20	3	750	8000
24	100-10.34-1000	600	29	3	2000	20	3	1000	8000
25	200-4.62-100	600	65	1	3800	19	4	100	15000
26	200-4.62-450	600	65	1	3800	19	4	450	15000
27	200-4.62-750	600	65	1	3800	19	4	750	15000
28	200-4.62-1000	600	65	1	3800	19	4	1000	15000
29	200-8.33-100	750	45	2	3800	19	4	100	18000
30	200-8.33-450	750	45	2	3800	19	4	450	18000
31	200-8.33-750	750	45	2	3800	19	4	750	18000
32	200-8.33-1000	750	45	2	3800	19	4	1000	18000
33	200-10.59-100	900	42.5	3	3800	19	4	100	21000
34	200-10.59-450	900	42.5	3	3800	19	4	450	21000
35	200-10.59-750	900	42.5	3	3800	19	4	750	21000
36	200-10.59-1000	900	42.5	3	3800	19	4	1000	21000

* Specimen ID is defined as (*h/w-b/2t-R*), where *R* is in metres.

The fabrication procedure was the same for all girders. The web and flange plates were assumed to be flame-cut. The resulting residual stresses were included in the models. The

residual stresses depend on the plate dimensions. They were calculated as described in Chapter 3. The residual stresses that were applied to the model as initial longitudinal, or tangential, stresses are shown in Table 4-2 and Table 4-3. Since the residual stresses are not a function of the radius of curvature, Table 4-2 defines the residual stresses for the different cross-sections of the models, namely, the "Specimen Group" shown in the table. The procedure for calculating the residual stresses shown in Table 4-2 and Table 4-3 was described in Section 3.6, and sample calculations are included in Appendix A.

Table 4-2: Flange plate residual stresses

Specimen Group	Tension at Each Flange Tip			Tension at Web Weld			Comp.
	Resultant	Width	Net per Element	Resultant	Width	Net per Element	
	F_y[1] (MPa)	c_f[1] (mm)	(MPa)	F_y[1] (MPa)	c_w[1] (mm)	(MPa)	σ_c[1*] (MPa)
075-4.61	350.0	13.7	231.9	350.0	17.5	350.0	194.0
075-8.33	350.0	14.4	63.0	350.0	35.0	350.0	137.7
075-10.63	350.0	14.1	43.0	350.0	36.3	283.1	108.7
100-4.62	350.0	21.3	127.0	350.0	25.0	165.4	97.4
100-8.33	350.0	14.4	63.0	350.0	35.0	350.0	137.7
100-10.34	350.0	16.9	52.0	350.0	30.2	143.5	65.2
200-4.62	350.0	25.3	110.6	350.0	21.3	82.4	64.4
200-8.33	350.0	21.1	63.2	350.0	24.9	83.7	49.0
200-10.59	350.0	20.5	48.9	350.0	25.6	70.8	39.9

[1] Refer to Figure 3-5.
[*] Remaining 6 of 10 elements in each flange were initialized with a constant compressive residual stress.

Table 4-3: Web plate residual stresses

Specimen Group	Tension at Top of Web			Tension at Bottom of Web			Comp.
	Resultant	Height	Net per Element	Resultant	Height	Net per Element	
	F_y[1] (MPa)	c_{fw}[1] (mm)	(MPa)	F_y[1] (MPa)	c_{fw}[1] (mm)	(MPa)	σ_c[1*] (MPa)
075-4.61	350.0	36.4	247.7	350.0	36.4	247.7	27.5
075-8.33	350.0	34.3	232.3	350.0	34.3	232.3	25.8
075-10.63	350.0	35.4	239.7	350.0	35.4	239.7	26.6
100-4.62	350.0	19.3	62.1	350.0	19.3	62.1	6.9
100-8.33	350.0	34.3	232.3	350.0	34.3	232.3	25.8
100-10.34	350.0	24.6	79.6	350.0	24.6	79.6	8.8
200-4.62	350.0	16.5	27.5	350.0	16.5	27.5	3.1
200-8.33	350.0	19.6	32.9	350.0	19.6	32.9	3.7
200-10.59	350.0	20.3	33.9	350.0	20.3	33.9	3.8

[1] Refer to Figure 3-5.
[*] Remaining 18 of 20 elements in the web were initialized with a constant compressive residual stress.

The specimens consisted of a simply supported span with load points at the points of lateral bracing, located at equal distance from the end vertical supports. Because the end segments are subjected to a more favorable moment distribution than the middle segment, they tend to provide lateral torsional buckling restraint to the middle segment, unless their length is increased. The effect of end segments restraint onto the middle segment was minimized by calculating the end segment length used for each model by equating the lateral torsional buckling moment in the end span to that of the middle segment, as described in Chapter 3. For the first models created, it was found that when using $\omega_2 = 1.75$ to calculate the end segment moment resistance resulted in end segments weaker than the middle segment. Since the middle segment is the portion of the girder under consideration, ω_2 needed to be adjusted to ensure that buckling of the middle segment took place at about the same time as buckling of the end segments. Using trial and error during the first model runs it was determined that $\omega_2 = 1.19$ for the end segments was appropriate to ensure the middle span buckled first. For some of the larger girder cross-sections, the end spans buckled first using the constant $\omega_2 = 1.19$. The models were reanalyzed with an ω_2 factor of 1.0, which meant the middle and end spans were the same length. The end span length used for each model is shown in Table 4-4. Similar to the tables showing the residual stresses, the radius of curvature is not required for the calculation of the end span length, thus the specimens were grouped together.

Table 4-4: End span lengths

Specimen Group	Middle Span Length	End Span Length Calculation	
	L (mm)	ω_2	L (mm)
075-4.61	8000	1.19	8992
075-8.33	8000	1.19	8801
075-10.63	8000	1.19	8774
100-4.62	8000	1.19	8781
100-8.33	8000	1.19	8750
100-10.34	8000	1.19	8742
200-4.62	15000	1.00*	15000
200-8.33	18000	1.00*	18000
200-10.59	21000	1.00*	21000

* End spans buckled first when using $\omega_2 = 1.19$.

To meet the requirements for the straight girder provisions of CSA-S6-06, partial-depth intermediate stiffeners were required for the models with $h/w = 200$. The partial depth stiffeners were added at one-third points, between the lateral support locations. Unlike the full-depth stiffeners at the load and support locations, these stiffeners were assumed to be welded to the web and top (compression) flange only, thus the bottom flange was able to rotate with respect to the web at the partial-depth stiffener locations.

The varied parameters included the flange width-to-thickness ratio, the web depth-to-thickness ratio and the radius of curvature. The girder specimens modeled are shown in Table 4-1. The range of radius of curvature was determined based on typical horizontal alignment requirements found in highway design guides and exceeding those guidelines to include girders with a radius as small as 100 m. Table 4-5 shows the actual moment resistance, M_r, of the parametric models compared to the yield moment, M_y, of the girder section.

Table 4-5: Moment resistance of parametric models

Model	Specimen ID	Flange Class	Web Class	Radius			
(#)	h/w - $b/2t$ -R			(m)	M_r (kN·m)	M_y (kN·m)	$\frac{M_r}{M_y}$
1	075-4.61-100	1	2	100	414	1904	0.22
2	075-4.61-450	1	2	450	454	1904	0.24
3	075-4.61-750	1	2	750	482	1904	0.25
4	075-4.61-1000	1	2	1000	485	1904	0.25
5	075-8.33-100	2	2	100	1800	3280	0.55
6	075-8.33-450	2	2	450	2158	3280	0.66
7	075-8.33-750	2	2	750	2212	3280	0.67
8	075-8.33-1000	2	2	1000	2236	3280	0.68
9	075-10.63-100	3	2	100	2488	3678	0.68
10	075-10.63-450	3	2	450	2866	3678	0.78
11	075-10.63-750	3	2	750	2946	3678	0.80
12	075-10.63-1000	3	2	1000	2992	3678	0.81
13	100-4.62-100	1	3	100	12220	17940	0.68
14	100-4.62-450	1	3	450	14690	17940	0.82
15	100-4.62-750	1	3	750	15050	17940	0.84
16	100-4.62-1000	1	3	1000	15190	17940	0.85
17	100-8.33-100	2	3	100	11040	14940	0.74
18	100-8.33-450	2	3	450	12920	14940	0.86
19	100-8.33-750	2	3	750	13260	14940	0.89
20	100-8.33-1000	2	3	1000	13450	14940	0.90
21	100-10.34-100	3	3	100	14090	16610	0.85
22	100-10.34-450	3	3	450	16150	16610	0.97
23	100-10.34-750	3	3	750	16530	16610	1.00
24	100-10.34-1000	3	3	1000	16700	16610	1.01
25	200-4.62-100	1	4	100	28320	66740	0.42
26	200-4.62-450	1	4	450	41910	66740	0.63
27	200-4.62-750	1	4	750	44290	66740	0.66
28	200-4.62-1000	1	4	1000	45670	66740	0.68
29	200-8.33-100	2	4	100	23590	60180	0.39
30	200-8.33-450	2	4	450	36980	60180	0.61
31	200-8.33-750	2	4	750	39760	60180	0.66
32	200-8.33-1000	2	4	1000	40840	60180	0.68
33	200-10.59-100	3	4	100	25520	66140	0.39
34	200-10.59-450	3	4	450	41460	66140	0.63
35	200-10.59-750	3	4	750	45340	66140	0.69
36	200-10.59-1000	3	4	1000	46930	66140	0.71

4.4 Results

The equations investigated were described in Chapter 2. They are Equations 2.20, 2.11 and 2.18 from and S6-14, AASHTO and S6-06, respectively.

$$\frac{M_{fx}}{M_{rx}} + U_c \frac{w_c M_{fw}}{M_{ry}} \leq 1 \quad [2.20]$$

$$f_{bu} + A \frac{1}{3} f_l \leq \phi_f F_{nc} \quad [2.11]$$

$$M_{fx} \leq M'_{rx} \quad [2.18]$$

Equations 2.20 and 2.11 include amplification factors, U_c and A, respectively. These amplification factors are used when a first-order analysis is conducted. When a second-order analysis is conducted, this amplification factor is 1.0 because the second-order effects are included in the analysis. As discussed in Chapter 2, in order to ensure the second-order effects of horizontally curved girders are properly accounted for, the analysis must contain nodes between points of lateral support (*i.e.*, cross-frames) and the cross-section must be modeled with either shell elements or a combination of shell and beam elements (such as the models used in the CISC design examples (CISC 2010)) to account for the second-order effects on lateral bending. The lateral bending stresses vary between points of lateral support, therefore, to correctly model the second-order stresses, there needs to be at least one node at the midpoint between cross-frames. Equation 2.18, used in CSA S6-06, was developed in the 1970s. It was intended for first-order analyses and does not include provisions for a second-order analysis.

Sample calculations to determine the moment resistance using the above equations are shown in Appendix A. Table 4-6 and Table 4-7 show the parametric analysis results and the associated calculated resistances for the first-order and second-order analyses, respectively. Even though the S6-06 equation was not intended for second-order analyses, a second-order analysis was conducted to compare the results of the interaction equation presented in S6-06 with and without second-order effects. The average and coefficient of variation (COV) for the calculated-to-FEA ratio for each equation are summarized as follows:

First-Order Analyses

S6-14 Average = 0.88, COV = 0.12

AASHTO Average = 0.74, COV = 0.18

S6-06 Average = 0.92, COV = 0.44

Second-Order Analyses

S6-14 Average = 0.95, COV = 0.10

AASHTO Average = 0.84, COV = 0.18

S6-06 Average = 0.79, COV = 0.28

Table 4-6: First-order analysis results of parametric study

Model	Specimen ID		S6-14 [2.20]		AASHTO [2.11]		S6-06 [2.18]	
(#)	h/w - $b/2t$ -R	M_r* (kN·m)	M_{calc} (kN·m)	$\frac{M_{calc}}{M_r}$	M_{calc} (kN·m)	$\frac{M_{calc}}{M_r}$	M_{calc} (kN·m)	$\frac{M_{calc}}{M_r}$
1	075-4.61-100	414	284	0.69	148	0.36	257	0.62
2	075-4.61-450	454	325	0.72	200	0.44	821	1.81
3	075-4.61-750	482	333	0.69	216	0.45	989	2.05
4	075-4.61-1000	485	337	0.69	220	0.45	1066	2.20
5	075-8.33-100	1800	1733	0.96	1564	0.87	1057	0.59
6	075-8.33-450	2158	2092	0.97	1926	0.89	2284	1.06
7	075-8.33-750	2212	2149	0.97	2019	0.91	2540	1.15
8	075-8.33-1000	2236	2207	0.99	2062	0.92	2643	1.18
9	075-10.63-100	2488	2286	0.92	2041	0.82	1388	0.56
10	075-10.63-450	2866	2843	0.99	2492	0.87	2738	0.96
11	075-10.63-750	2946	2948	1.00	2597	0.88	3018	1.02
12	075-10.63-1000	2992	2977	0.99	2635	0.88	3114	1.04
13	100-4.62-100	12220	11680	0.96	9715	0.80	6640	0.54
14	100-4.62-450	14690	13870	0.94	11940	0.81	13170	0.90
15	100-4.62-750	15050	14290	0.95	12390	0.82	14610	0.97
16	100-4.62-1000	15190	14460	0.95	12740	0.84	15150	1.00
17	100-8.33-100	11040	10700	0.97	8534	0.77	6144	0.56
18	100-8.33-450	12920	12520	0.97	10430	0.81	11550	0.89
19	100-8.33-750	13260	12880	0.97	10780	0.81	12600	0.95
20	100-8.33-1000	13450	13090	0.97	11010	0.82	13090	0.97
21	100-10.34-100	14090	13010	0.92	10490	0.74	7835	0.56
22	100-10.34-450	16150	15370	0.95	12590	0.78	13410	0.83
23	100-10.34-750	16530	15700	0.95	13020	0.79	14360	0.87
24	100-10.34-1000	16700	15950	0.96	13260	0.79	14940	0.89
25	200-4.62-100	28320	25400	0.90	19690	0.70	9987	0.35
26	200-4.62-450	41910	32760	0.78	27300	0.65	34440	0.82
27	200-4.62-750	44290	34650	0.78	29250	0.66	42300	0.96
28	200-4.62-1000	45670	35190	0.77	30430	0.67	46120	1.01
29	200-8.33-100	23590	22000	0.93	17160	0.73	7248	0.31
30	200-8.33-450	36980	29160	0.79	24730	0.67	28420	0.77
31	200-8.33-750	39760	30890	0.78	26530	0.67	36430	0.92
32	200-8.33-1000	40840	31680	0.78	27720	0.68	40000	0.98
33	200-10.59-100	25520	22460	0.88	19930	0.78	7060	0.28
34	200-10.59-450	41460	31930	0.77	29530	0.71	29530	0.71
35	200-10.59-750	45340	34400	0.76	31750	0.70	38370	0.85
36	200-10.59-1000	46930	35580	0.76	32800	0.70	42510	0.91
			Average	0.88		0.74		0.92
			Coefficient of Variation	0.12		0.18		0.44

* Value obtained from the finite element analysis.

Table 4-7: Second-order analysis results of parametric study

Model	Specimen ID		S6-14 [2.20]		AASHTO [2.11]		S6-06 [2.18]	
(#)	h/w - $b/2t$ -R	M_r* (kN·m)	M_{calc} (kN·m)	$\frac{M_{calc}}{M_r}$	M_{calc} (kN·m)	$\frac{M_{calc}}{M_r}$	M_{calc} (kN·m)	$\frac{M_{calc}}{M_r}$
1	075-4.61-100	414	321	0.78	173	0.42	216	0.52
2	075-4.61-450	454	355	0.78	236	0.52	448	0.99
3	075-4.61-750	482	359	0.74	247	0.51	457	0.95
4	075-4.61-1000	485	359	0.74	252	0.52	460	0.95
5	075-8.33-100	1800	1989	1.11	1818	1.01	991	0.55
6	075-8.33-450	2158	2283	1.06	2201	1.02	2173	1.01
7	075-8.33-750	2212	2344	1.06	2279	1.03	2442	1.10
8	075-8.33-1000	2236	2352	1.05	2294	1.03	2556	1.14
9	075-10.63-100	2488	2521	1.01	2440	0.98	1332	0.54
10	075-10.63-450	2866	2983	1.04	2842	0.99	2667	0.93
11	075-10.63-750	2946	3053	1.04	2878	0.98	2948	1.00
12	075-10.63-1000	2992	3114	1.04	2909	0.97	3080	1.03
13	100-4.62-100	12220	12930	1.06	11610	0.95	6385	0.52
14	100-4.62-450	14690	14750	1.00	13690	0.93	12990	0.88
15	100-4.62-750	15050	14920	0.99	13970	0.93	14290	0.95
16	100-4.62-1000	15190	14970	0.99	14110	0.93	14970	0.99
17	100-8.33-100	11040	11540	1.05	10310	0.93	5910	0.54
18	100-8.33-450	12920	13070	1.01	11820	0.91	11270	0.87
19	100-8.33-750	13260	13160	0.99	12040	0.91	12460	0.94
20	100-8.33-1000	13450	13390	1.00	12200	0.91	12790	0.95
21	100-10.34-100	14090	13540	0.96	12700	0.90	7690	0.55
22	100-10.34-450	16150	15690	0.97	14220	0.88	13240	0.82
23	100-10.34-750	16530	15860	0.96	14360	0.87	14360	0.87
24	100-10.34-1000	16700	16120	0.97	14440	0.86	14770	0.88
25	200-4.62-100	28320	28980	1.02	22080	0.78	9391	0.33
26	200-4.62-450	41910	37300	0.89	31750	0.76	30930	0.74
27	200-4.62-750	44290	38750	0.87	33630	0.76	38330	0.87
28	200-4.62-1000	45670	39110	0.86	34130	0.75	42230	0.92
29	200-8.33-100	23590	25080	1.06	19180	0.81	6992	0.30
30	200-8.33-450	36980	33150	0.90	28610	0.77	25720	0.70
31	200-8.33-750	39760	34910	0.88	30400	0.76	32290	0.81
32	200-8.33-1000	40840	35370	0.87	31210	0.76	35370	0.87
33	200-10.59-100	25520	24570	0.96	22230	0.87	6798	0.27
34	200-10.59-450	41460	36340	0.88	33690	0.81	27040	0.65
35	200-10.59-750	45340	38520	0.85	35990	0.79	34710	0.77
36	200-10.59-1000	46930	39890	0.85	36800	0.78	38120	0.81
			Average	0.95		0.84		0.79
			Coefficient of Variation	0.10		0.18		0.28

* Value obtained from the finite element analysis.

4.5 Discussion

Models 1 to 4 in Table 4-5 have actual moment resistances, M_r, that are less than 30% of the yield moment, M_y. The objective of this study was to develop a database of curved girders with moment capacities less than 80% of M_y . However, using member dimensions with a flexural resistance of only 30% of M_y is unrealistic for girders that would typically be used in highway bridges. The 075-4.61 specimens have web depths of 1000 mm and flange widths of 175 mm, with an unbraced length of 8000 mm. These member dimensions would not be typical for highway bridges. Referring to Table 4-6 and Table 4-7, all three equations perform poorly for these four models for both first and second-order analyses. In addition, for these four models, the calculated-to-FEA moment ratios for S6-14 and AASHTO equations are significantly lower than for the remaining data set. The average calculated-to-FEA ratios for the S6-14 and AASHTO first-order analyses are 0.88 and 0.78, respectively. The average ratios for Models 1 to 4 for those equations are 0.70 and 0.43, respectively. The second-order analyses for S6-14 and AASHTO have a similar reduction in accuracy for those four models. For S6-06, the calculated-to-FEA ratio varies significantly, from 0.62 to 2.20 for the first-order analysis. However, the second-order analysis the results are close to 1.0, which is desirable, except for Model 1, which was 0.52. However, as discussed previously, the S6-06 equation was not intended to be used with second-order analyses. Based on this information it is justified to exclude these models when assessing the performance of the equations being investigated. Figure 4-1 and Figure 4-2 show the calculated-to-FEA moment ratio for each equation excluding the 075-4.61 models, for the first-order and second-order analyses respectively. The revised average and coefficient of variation (COV) for the calculated-to-FEA ratio for each equation are summarized as follows:

First-Order Analyses

S6-14 Average = 0.90, COV = 0.10

AASHTO Average = 0.78, COV = 0.10

S6-06 Average = 0.82, COV = 0.28

Second-Order Analyses

S6-14 Average = 0.98, COV = 0.08

AASHTO Average = 0.89, COV = 0.10

S6-06 Average = 0.78, COV = 0.29

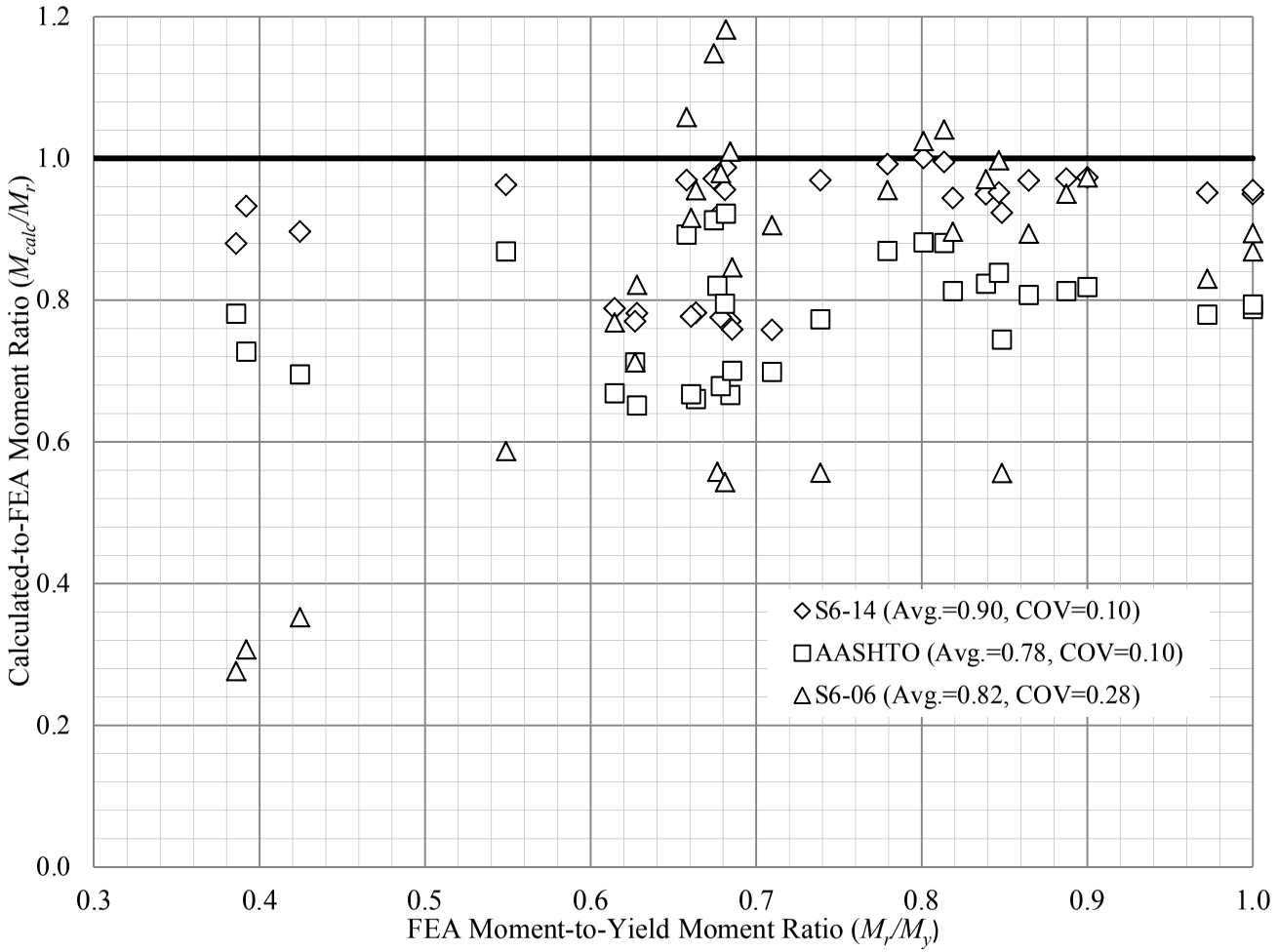

Figure 4-1: Performance of first-order analysis equations

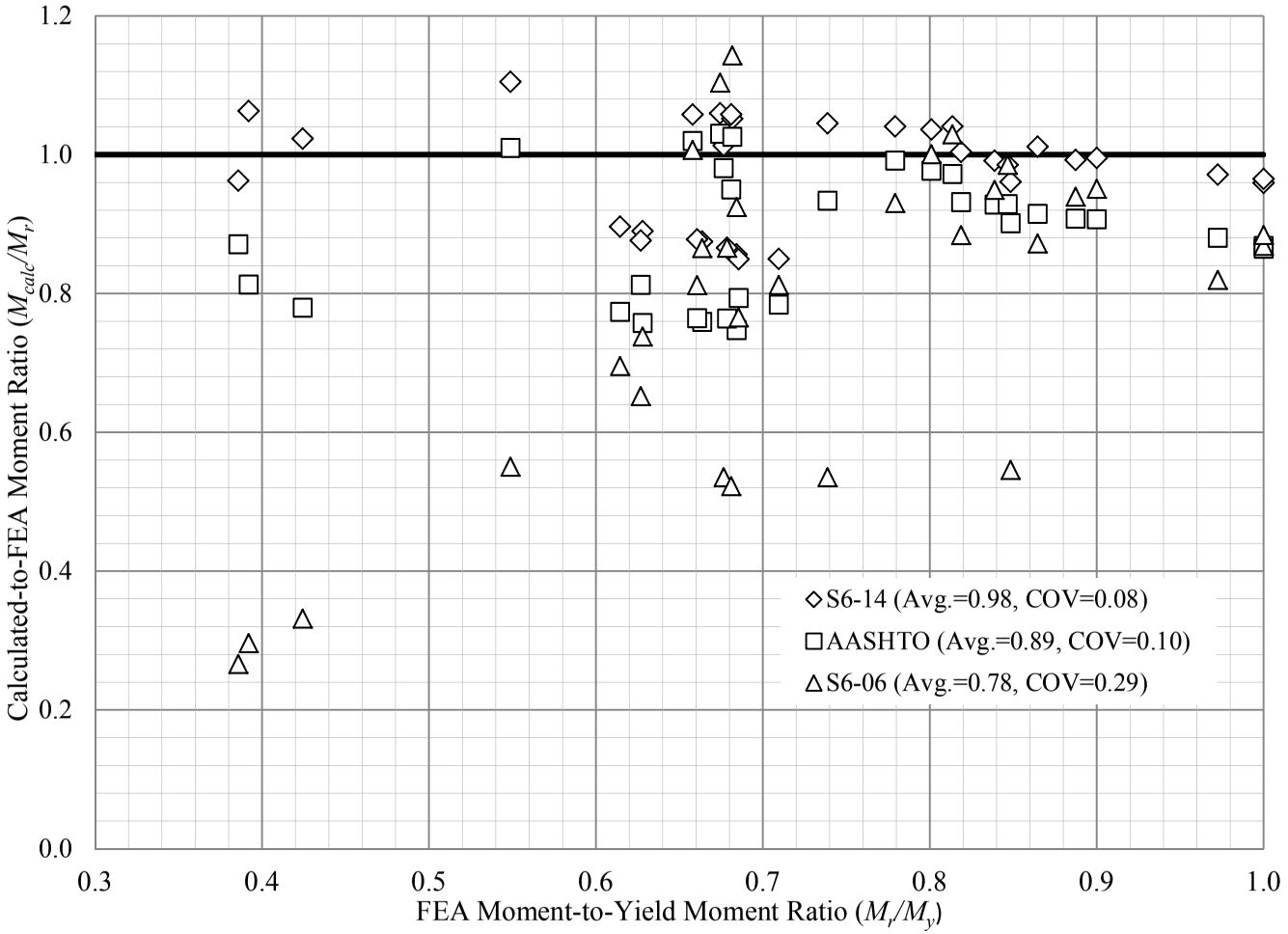

Figure 4-2: Performance of second-order analysis equations

The varied parameters were the radius of curvature, flange width-to-thickness ratio, and web height-to-thickness ratio. Table 4-8, Table 4-9, and Table 4-10 show the sensitivity of each of these parameters. These tables exclude the results from the 075-4.61 models.

Table 4-8: Average calculated-to-FEA moment ratio for various radii of curvature

Radius	S6-14 [2.21]		AASHTO [2.12]		S6-06 [2.18]	
R (m)	1st Order	2nd Order	1st Order	2nd Order	1st Order	2nd Order
100	0.93	1.03	0.78	0.91	0.47	0.45
450	0.90	0.97	0.77	0.89	0.87	0.83
750	0.90	0.96	0.78	0.88	0.96	0.91
1000	0.90	0.95	0.79	0.87	1.00	0.95

Table 4-9: Average calculated-to-FEA moment ratio for various *b/2t* ratios

	S6-14 [2.21]		AASHTO [2.12]		S6-06 [2.18]	
b/2t	1st Order	2nd Order	1st Order	2nd Order	1st Order	2nd Order
4.6	0.88	0.96	0.74	0.85	0.82	0.78
8.3	0.92	1.00	0.80	0.91	0.86	0.81
10.6	0.90	0.96	0.79	0.89	0.79	0.76

Table 4-10: Average calculated-to-FEA moment ratio for various *h/w* ratios

	S6-14 [2.21]		AASHTO [2.12]		S6-06 [2.18]	
h/w	1st Order	2nd Order	1st Order	2nd Order	1st Order	2nd Order
75	0.98	1.05	0.88	1.00	0.94	0.91
100	0.96	1.00	0.80	0.91	0.83	0.81
200	0.81	0.91	0.69	0.79	0.74	0.67

Referring to Table 4-8, Table 4-9, and Table 4-10 the average calculated-to-FEA moment ratio for the S6-14 second-order analysis increases to above 1.0 as the radius is decreased to 100 m. In addition, for the S6-14 first-order analysis, the ratio increases to 0.930 for the 100 m radii models, after remaining constant at 0.90 for the 450, 750, and 1000 m radii models. The S6-14 and AASHTO analyses appear to have constant or slightly increasing average ratios as the radius decreases. Whereas both S6-06 equations decrease as the radius is decreased. The average calculated-to-FEA moment appears to remain constant for all first and second-order analyses as the flange width-to-thickness ratio is varied. The average ratio increases as the web slenderness, h/w, is decreased.

CHAPTER 5

CONCLUSIONS AND RECOMMENDATIONS

5.1 Summary

The past two decades have seen an increase in usage of horizontally curved steel I-girders for highway bridges. With the increased availability of structural analysis software, the analysis of horizontally curved bridges has become relatively simple, but the design provisions in the Canadian Highway Bridge Design Code for this type of bridges have fallen behind the current state of knowledge in this area. This research project was conducted to help provide direction for the development of updated design provisions for CSA-S6.

Although there has been extensive research done into the behaviour of horizontally curved steel I-girders, a review of the available analysis and experimental data revealed that there were limited data for girders failing by lateral torsional buckling at moments less than 80% of their yield moment. Elastic and inelastic lateral torsional buckling failures typically occur below 80% of the beam's yield moment.

To address the lack of available information on elastic and inelastic lateral torsional buckling of horizontally curved girders, a numerical parametric study was developed to supplement the research database. The finite element model developed was validated by comparing with previous experimental and numerical analyses. A total of 36 single girder models were created and loaded under uniform bending. The maximum moment capacity of these models varied between 22 and 100% of the yield moment. The varied parameters included the radius of curvature, the flange width-to-thickness ratio, and the web height-to-thickness ratio. The radius of curvature, R, varied from 100 to 1000 m. The flange width-to-thickness ratio, $b/2t$, varied from 4.6 to 10.6. The web height-to-thickness ratio, h/w, varied from 75 to 200.

Different curved girder design equations were explored, and three were chosen to be investigated. The calculated first and second-order design equations used in

CAN/CSA-S6-06, S6-14, and AASHTO were compared with the actual moment resistances found from the models to determine which equation performed best.

5.2 Conclusions and Design Recommendations

The proposed equation for CAN/CSA-S6-14 performed better than the current S6-06 version and the AASHTO equation, with mean predicted-to-FE analysis result ratio of 0.90 and COV of 0.10 for the first-order analyses, 0.98 and 0.08 respectively, for the second-order analyses. The equations for S6-14 had the best average between predicted and actual moment resistance and the lowest coefficient of variation for both the first and second-order analyses. In addition to that, the average for the first-order analyses was only slightly lower than for the second-order analyses, meaning designers are not penalized for using a simpler first-order analysis.

The following equation is recommended for the design of horizontally curved steel I-girders:

$$\frac{M_{fx}}{M_{rx}} + U_c \frac{w_c M_{fw}}{M_{ry}} \leq 1 \qquad [2.20]$$

where w_c is taken as 0.5 for horizontally curved girders, and the moment amplification factor, U_c, is taken as 1.0 when the factored moments M_{fx} and M_{fw} are obtained from a second-order analysis. When M_{fx} and M_{fw} are obtained from a first-order analysis, U_c, is taken as the following:

$$U_c = \left(\frac{0.85}{1 - M_{fx}/M_u} \right)$$

5.3 Recommendations for Further Research

This parametric study did not explore I-girders with a radius of curvature smaller than 100 m. Highway bridges have been designed with radii smaller than 100 m. In addition, for the S6-14 equation, the predicted-to-test ratio exceeded 1.0 for the 100 m radii models, which is unconservative. It is therefore recommended that further research be conducted on horizontally curved girders with smaller radii.

A reliability analysis was not within the scope of this research project. Although a reliability analysis was conducted during the development of the 2014 edition of S6, the analysis should be updated with the expanded database of results now available.

REFERENCES

American Association of State Highway and Transportation Officials (AASHTO). (1980). *Guide specifications for horizontally curved highway bridges.* Washington, DC.

American Association of State Highway and Transportation Officials (AASHTO). (1993). *Guide specifications for horizontally curved highway bridges*. Washington, DC.

American Association of State Highway and Transportation Officials (AASHTO). (2003). *Guide specifications for horizontally curved highway bridges*. Washington, DC.

American Association of State Highway and Transportation Officials (AASHTO). (2004). *AASHTO LRFD bridge design specifications. 3rd Ed., with 2006 Interims*. Washington, DC.

American Association of State Highway and Transportation Officials (AASHTO). (2012). *AASHTO LRFD bridge design specifications. 6th Ed.* Washington, DC.

Canadian Institute of Steel Construction (CISC). (2010). *Steel bridges – Design, fabrication, construction. Curved plate girder bridge: Design example 3*. Markham, ON.

Canadian Standards Association (CSA). (2012). *CAN/CSA-S6-06 Canadian highway bridge design code. Reaffirmed 2012.* Mississauga, ON.

Canadian Standards Association (CSA). (2014). *CAN/CSA-S6-14 Canadian highway bridge design code. Draft*. Mississauga, ON.

Dassault Systemes Simulia Corporation. (2012). *Abaqus 6.12 analysis user's manual*. Providence, RI.

Davidson, J. S. (1992). "Nominal bending and shear strength of horizontally curved steel-I-girder bridges." Ph.D. dissertation, Auburn Univ., Auburn, AL.

Davidson, J. S., Ballance, S. R., and Yoo, C. H. (1999a). "Analytical model of curved I-girder web panels subjected to bending." *J. Bridge Eng.*, 4(3), 204–212.

Davidson, J. S., Ballance, S. R., and Yoo, C. H. (1999b). "Finite displacement behavior of curved I-girder webs subjected to bending." *J. Bridge Eng.*, 4(3), 213–220.

European Convention for Conventional Steelwork (ECCS). (1976). "Manual on stability of steel structures." *Pub. No. 22, Committee 8-Stability, 2nd Ed.*, Brussels, Belgium.

Grondin, G. Y., Chen, Q., Elwi, A. E., and Cheng, J. J. (1998). "Stiffened steel plates under compression and bending*." J. Construct. Steel Res.*, 45(2), 125–148.

Hartmann, J. L. (2005). "An experimental investigation of the flexural resistance of horizontally curved steel I-girder systems." Ph.D. dissertation, Univ. of Maryland, College Park, MD.

Jung, S.-K. (2006). "Inelastic strength and behavior of horizontally curved composite I-girder bridge structural system." Ph.D. thesis, Georgia Institute of Technology, Atlanta, GA.

McManus, P. F. (1971). "Lateral buckling of curved plate girders." Ph.D. thesis, Carnegie-Mellon Univ., Pittsburgh, PA.

Mozer, J., Cook, J., and Culver, C. (1973). "Horizontally curved highway bridges-Stability of curved plate girders." *Rep. No. P3, Research Project HPR-2(111)*, Carnegie-Mellon Univ., Pittsburgh, PA.

Mozer, J., and Culver, C. (1970). "Horizontally curved highway bridges-Stability of curved plate girders." *Rep. No. P1, Research Project HPR-2(111)*, Carnegie-Mellon Univ., Pittsburgh, PA.

Mozer, J., Ohlson, R., and Culver, C. (1971). "Horizontally curved highway bridges-Stability of curved plate girders." *Rep. No. P2, Research Project HPR-2(111)*, Carnegie-Mellon Univ., Pittsburgh, PA.

Nakai, H., and Kotoguchi, H. (1983). "A study on lateral buckling strength and design aid for horizontally curved I-girder bridges." *Proc., Applied Mechanics and Structure Engineering Division, Japanese Society of Civil Engineers*, 195–205.

Nakai, H., and Yoo, C. H. (1988). "Analysis and design of curved steel bridges." McGraw-Hill, New York, NY.

National Cooperative Highway Research Program (NCHRP). (1999). “Improved design specifications for horizontally curved steel girder highway bridges.” *Rep. No. 424, Transportation Research Board*, Washington, DC.

National Cooperative Highway Research Program (NCHRP). (2006). “Development of LRFD specifications for horizontally curved steel girder bridges.” *Rep. No. 563, Transportation Research Board*, Washington, DC.

Schumacher, A., Grondin, G. Y., and Kulak, G. L. (1997). “Connection of infill panels in steel plate shear walls.” *Structural Engineering Report No. 217*, University of Alberta, Edmonton, AB.

Shanmugam, N., Thevendran, V., Liew, J., and Tan, L. (1995). “Experimental study on steel beams curved in plan.” *J. Struct. Eng.*, 121(2), 249–259.

White, D. W., and Grubb, M. A. (2005). “Unified Resistance Equations for Design of Curved and Tangent Steel Bridge I-Girders.” *J. Transportation Res. Board*, CD 11-S, 121–128.

White, D. W., Zureick, A. H., Phoawanich, N., and Jung, S.-K. (2001). “Development of unified equations for design of curved and straight steel bridge I girders.” *Final Report to American Iron and Steel Institute Transportation and Infrastructure Committee, Professional Services Inc., FHWA*, Georgia Institute of Technology, Atlanta, GA.

Yoo, C. H., Kang, Y. J., and Davidson, J. S. (1996). “Buckling analysis of curved beams by finite-element discretization.” *J. Eng. Mech.*, 122(8), 762–770.

APPENDIX A

SAMPLE CALCULATIONS

MOMENT RESISTANCE OF STRAIGHT MEMBER

Sample calculation for model 075-8.33-100

Girder Dimensions:

b = 350 mm

t = 21 mm

h = 1000 mm

w = 13.3 mm

L = 8000 mm

Girder Properties:

F_y = 350 MPa

E = 200 000 MPa

G = 77 000 MPa

I_x = 4.784×10^9 mm^4

I_y = 150.3×10^6 mm^4

C_w = 37.52×10^{12} mm^6

J = 2.945×10^6 mm^4

S_x = 9.371×10^6 mm^3

Calculations:

1. Determine yield moment, M_y

$$M_y = F_y S_x$$
$$= (350MPa)(9.371 \text{x} 10^6 \text{ mm}^3)$$
$$= 3280kNm$$

2. Determine elastic buckling moment resistance, M_u for the middle span under uniform bending moment $(\omega_2 = 1.0)$.

$$M_u = \frac{w_2 \pi}{L} \sqrt{EI_y GJ + \left(\frac{\pi E}{L}\right)^2 I_y C_w}$$

$$EI_y GJ = (200000MPa)(150.3x10^6 mm^4)(77000MPa)(2.945x10^6 mm^4)$$
$$= 6.817x10^{24} MPa^2 mm^8$$

$$\left(\frac{\pi E}{L}\right)^2 I_y C_w = \left(\frac{\pi(200000MPa)}{(8000mm)}\right)^2 (150.3x10^6 mm^4)(37.52x10^{12} mm^6)$$
$$= 3.479^{25} MPa^2 mm^8$$

$$M_u = \frac{(1.0)\pi}{(8000mm)} \sqrt{(6.817 \text{x} 10^{24} \text{ MPa}^2\text{mm}^8) + (3.479 \text{x} 10^{25} \text{ MPa}^2\text{mm}^8)}$$
$$= 2532kNm$$

3. Determine inelastic buckling moment resistance, M_{ui}

$$M_{ui} = 1.15M_y \left(1 - \frac{0.28M_y}{M_u}\right)$$
$$= 1.15(3280kNm)\left(1 - \frac{0.28(3280kNm)}{(2532kNm)}\right)$$
$$= 2404kNm$$

M_{ui}<M_u<M_y therefore, M_r = 2404 kNm.

END SPAN LENGTH CALCULATION

Sample calculation for model 075-8.33-100

Girder Dimensions:

b = 350 mm

t = 21 mm

h = 1000 mm

w = 13.3 mm

L = 8000 mm

Girder Properties:

F_y = 350 MPa

E = 200 000 MPa

G = 77 000 MPa

I_x = 4.784×10^9 mm^4

I_y = 150.3×10^6 mm^4

C_w = 37.52×10^{12} mm^6

J = 2.945×10^6 mm^4

S_x = 9.371×10^6 mm^3

Given:

M_y = 3280 kNm (from previous sample calculation)

M_r = 2404 kNm (from previous sample calculation)

Calculations:

1. Using trial and error, determine what end span length using $\omega_2 = 1.75$ (moment gradient) gives an equivalent moment resistance to the middle span, $M_r = 2404kNm$, calculated in the previous sample calculation.

Try $L = 10942mm$:

$$M_u = \frac{w_2\pi}{L}\sqrt{EI_yGJ + \left(\frac{\pi E}{L}\right)^2 I_yC_w}$$

$$EI_yGJ = (200000MPa)(150.3x10^6 mm^4)(77000MPa)(2.945x10^6 mm^4)$$
$$= 6.817x10^{24} MPa^2 mm^8$$

$$\left(\frac{\pi E}{L}\right)^2 I_yC_w = \left(\frac{\pi(200000MPa)}{(10942mm)}\right)^2 (150.3x10^6 mm^4)(37.52x10^{12} mm^6)$$
$$= 1.859^{25} MPa^2 mm^8$$

$$M_u = \frac{(1.75)\pi}{(10942mm)}\sqrt{(6.817\,x\,10^{24}\ \mathrm{MPa^2mm^8}) + (1.859\,x\,10^{25}\ \mathrm{MPa^2mm^8})}$$
$$= 2532kNm$$

$$M_{ui} = 1.15M_y\left(1 - \frac{0.28M_y}{M_u}\right)$$
$$= 1.15(3280kNm)\left(1 - \frac{0.28(3280kNm)}{(2532kNm)}\right)$$
$$= 2404kNm$$

M_{ui}=M_r = 2404 kNm, therefore using an endspan length of 10942 mm and middle span length of 8000 mm will eliminate the restraint that the end spans provide the middle span for a straight girder, under a 4-point bending load.

2. Using trial and error, determine what end span length using $\omega_2 = 1.19$ (modified moment gradient) gives an equivalent moment resistance to the middle span, $M_r = 2404kNm$, calculated in the previous sample calculation.

Try $L = 8801mm$:

$$M_u = \frac{w_2\pi}{L}\sqrt{EI_yGJ + \left(\frac{\pi E}{L}\right)^2 I_yC_w}$$

$$EI_yGJ = (200000MPa)(150.3x10^6 mm^4)(77000MPa)(2.945x10^6 mm^4)$$
$$= 6.817x10^{24} MPa^2 mm^8$$

$$\left(\frac{\pi E}{L}\right)^2 I_yC_w = \left(\frac{\pi(200000MPa)}{(8801mm)}\right)^2 (150.3x10^6 mm^4)(37.52x10^{12} mm^6)$$
$$= 2.874^{25} MPa^2 mm^8$$

$$M_u = \frac{(1.19)\pi}{(8801mm)}\sqrt{(6.817\,x\,10^{24}\ \mathrm{MPa^2 mm^8}) + (2.874\,x\,10^{25}\ \mathrm{MPa^2 mm^8})}$$
$$= 2532kNm$$

$$M_{ui} = 1.15M_y\left(1 - \frac{0.28M_y}{M_u}\right)$$
$$= 1.15(3280kNm)\left(1 - \frac{0.28(3280kNm)}{(2532kNm)}\right)$$
$$= 2404kNm$$

M_{ui}=M_r = 2404 kNm, therefore using an endspan length of 8801 mm and middle span length of 8000 mm will minimize the restraint that the end spans provide the middle span for a curved girder, under a 4-point bending load.

RESIDUAL STRESS CALCULATIONS (ECCS 1976)

Sample calculation for model 075-8.33-100

Plate dimensions:

b = 350 mm

t = 21 mm

h = 1000 mm

w = 13.3 mm

Given:

F_y = 350 MPa (plate yield strength)

p = 0.90 (process efficiency factor for submerged arc welding)

A_w = 32 mm^2 (area of an 8 mm fillet weld)

F = 35 mm (flange element width used in ABAQUS model)

W = 50 mm (web element height used in ABAQUS model)

Calculations:

1. Determine width of the tensile yield stress block, c_f, at the flange tips due to flame cutting.

$$c_f = \frac{1100\sqrt{t}}{F_y}$$

$$= \frac{1100\sqrt{(21mm)}}{(350MPa)}$$

$$= 14.4mm$$

2. Determine the width of the tensile yield stress block, c_w, in the flange at the weld location.

$$c_w = \frac{12000\,pA_w}{F_y \Sigma t}$$

$$= \frac{12000(0.90)(32mm^2)}{(350MPa)[(21mm)+(13.3mm)]}$$

$$= 28.8mm$$

3. The weld is actually located at the web face; therefore adjust c_w to be the distance from the centre of the flange to the extent of the tensile yield stress block.

$$c_w = \frac{w}{2} + c_w$$

$$= \frac{(13.3mm)}{2} + (28.8mm)$$

$$= 35.43mm$$

4. Note, the flange element width in the ABAQUS model is 35 mm, which is close to the calculated c_w. For ease of calculation of the ABAQUS input residual stresses, use $c_w = 35mm$.

$$c_w = 35.0mm$$

5. Determine the magnitude of the compressive residual stress block, σ_c, in the flange. The tensile residual stresses in the flange must be equilibrated with the compressive residual stresses.

$$\sigma_c = \frac{F_y\left(2c_f + 2c_w\right)}{b - 2c_f - 2c_w}$$

$$= \frac{(350MPa)\left[2(14.4mm)+2(35mm)\right]}{[(350mm)-2(14.4mm)-2(35mm)]}$$

$$= 137.7MPa$$

6. Because the width of the tension block is not equal to the actual flange element in the ABAQUS model, the magnitude of the tensile residual stresses must be adjusted.

   For the flange elements along the flange tip:

$$\sigma_{input} = \frac{F_y c_f - \sigma_c \left(F - c_f \right)}{F}$$

$$= \frac{(350MPa)(14.4mm) - (137.7MPa)[(35mm) - 14.4mm)]}{(35mm)}$$

$$= 63.0MPa$$

   For the flange elements at web-to-flange weld:

$$\sigma_{input} = \frac{F_y c_w - \sigma_c \left(F - c_w \right)}{F}$$

$$= \frac{(350MPa)(35.0mm) - (137.7MPa)[(35\,\mathrm{mm}) - (35.0mm)]}{(35mm)}$$

$$= 350.0MPa$$

7. Determine height of tensile yield stress block, c_f, at the top and bottom of the web due to flame cutting.

$$c_f = \frac{1100\sqrt{t}}{F_y}$$

$$= \frac{1100\sqrt{(13.3mm)}}{(350MPa)}$$

$$= 11.5mm$$

8. Determine height of tensile yield stress block, c_w, at the top and bottom of the web due to welding.

$$c_w = \frac{12000\,pA_w}{F_y \Sigma t}$$

$$= \frac{12000(0.90)(32mm^2)}{(350MPa)[(13.3mm)+(21mm)]}$$

$$= 28.8mm$$

9. c_w must be modified to account for multiple welds being deposited at each joint location.

$$c_w = 2^{1/4} c_w$$

$$= 2^{1/4}(28.8mm)$$

$$= 34.2mm$$

10. The web tips are flame-cut and then welded. Determine the height of the final tensile yield stress block at the top and bottom of the web.

$$c_{fw}^4 = \sqrt[4]{c_f^4 + c_w^4}$$

$$= \sqrt[4]{(11.5mm)^4 + (34.2mm)^4}$$

$$= 34.3mm$$

11. Determine the magnitude of the compressive residual stress block, σ_c, in the web. The tensile residual stresses in the web must be equilibrated with the compressive residual stresses.

$$\sigma_c = \frac{F_y\left(2c_{fw}\right)}{h - 2c_{fw}}$$

$$= \frac{(350MPa)\left(2(34.3mm)\right)}{(1000mm) - 2(34.3mm)}$$

$$= 25.8MPa$$

12. Because the tension block width is not equal to the actual element height of the web elements in the model, the magnitude of the tensile residual stresses must be adjusted.

    For the web elements along the top and bottom of the web:

$$\sigma_{input} = \frac{F_y c_{fw} - \sigma_c \left(W - c_{fw}\right)}{W}$$

$$= \frac{(350MPa)(34.3mm) - (25.8MPa)[(50\,\text{mm}) - (34.3mm)]}{(50mm)}$$

$$= 232.3MPa$$

Therefore, the calculated and initial model input stresses are shown in the tables below.

Table 4-1: Flange plate residual stresses

Specimen Group	Tension at Each Flange Tip			Tension at Web Weld			Comp.
	Resultant	Width	Net per Element	Resultant	Width	Net per Element	
	F_y[1] (MPa)	c_f[1] (mm)	(MPa)	F_y[1] (MPa)	c_w[1] (mm)	(MPa)	σ_c[1*] (MPa)
075-8.33	350.0	14.4	63.0	350.0	35.0	350.0	137.7

[1] Refer to Figure 3-5.
[*] Remaining 6 of 10 elements in each flange were initialized with a constant compressive residual stress.

Table 4-2: Web plate residual stresses

Specimen Group	Tension at Top of Web			Tension at Bottom of Web			Comp.
	Resultant	Height	Net per Element	Resultant	Height	Net per Element	
	F_y[1] (MPa)	c_{fw}[1] (mm)	(MPa)	F_y[1] (MPa)	c_{fw}[1] (mm)	(MPa)	σ_c[1*] (MPa)
075-8.33	350.0	34.3	232.3	350.0	34.3	232.3	25.8

[1] Refer to Figure 3-5.
[*] Remaining 18 of 20 elements in the web were initialized with a constant compressive residual stress.

CSA S6-14 FIRST-ORDER ANALYSIS EQUATION

Sample calculation for model 075-8.33-100

Girder Dimensions:

b = 350 mm

t = 21 mm

h = 1000 mm

w = 13.3 mm

L = 8000 mm

R = 100 m

Girder Properties:

F_y = 350 MPa

E = 200 000 MPa

G = 77 000 MPa

Given:

M_y = 3280 kNm (from previous sample calculation)

M_r = 2404 kNm (from previous sample calculation)

M_u = 2532 kNm (from previous sample calculation)

CSA S6-14 Design Equation:

Determine the maximum calculated vertical moment, M_{fx}, that satisfies the equation shown below:

$$\frac{M_{fx}}{M_r} + U_c \frac{w_c M_{fw}}{M_{ry}} \leq 1$$

M_{fx} = vertical bending moment (from the 1st order finite element model)

M_{fw} = lateral bending moment (from 1st order finite element model)

M_r = vertical bending moment resistance

= 2404 kNm (from previous sample calculation)

M_{ry} = lateral bending moment resistance

w_c = 0.5 for major lateral moment reversals between the lateral supports

U_c = $\left(\frac{0.85}{1 - \frac{M_{fx}}{M_u}} \right)$ = amplification factor for first-order analyses

Calculations:

1. Determine the lateral bending moment resistance, M_{ry}. Note that for this analysis the applied lateral bending moment, M_{fw}, was calculated for a single flange only and neglected the contribution from the web. Therefore, the lateral bending moment resistance is calculated using only the single flange.

   Model 075-8.33-100 uses Class 2 flanges. Therefore, the lateral bending moment resistance is equivalent to the plastic moment of the rectangular shape.

$$M_{ry} = \frac{b^2 t F_y}{4}$$

$$= \frac{(350mm)^2 (21mm)(350MPa)}{4}$$

$$= 225.1kNm$$

2. Use the analysis output to determine if the maximum calculated vertical moment has been reached. The analysis provided output for every 1% increase in vertical moment. The output data from a specific increment step was used to determine if the maximum calculated vertical moment had been reached.

   When $M_{fx} = 1733kNm$, the following longitudinal stresses were in the compression flange tips at the midspan between lateral supports:

σ_i = $287.6MPa$ in compression along the inside flange tip

σ_o = $67.7MPa$ in compression along the outside flange tip

3. Determine the lateral bending moment, M_{fw}, from the stresses at the flange tips.

f_{bu} = vertical bending stress

$$= \left|\frac{\sigma_i + \sigma_o}{2}\right|$$

$$= \left|\frac{(-287.6MPa) + (-67.7MPa)}{2}\right|$$

$$= 177.7MPa$$

f_l = lateral bending stress

$$= f_{bu} - |\sigma_o|$$

$$= (177.7MPa) - |(-67.7MPa)|$$

$$= 110.0MPa$$

M_{fw} = $\frac{f_l\left(\frac{b^3 t}{12}\right)}{(b/2)}$ for a linear stress distribution

$$= \frac{(110.0MPa)\left(\frac{(350mm)^3(21mm)}{12}\right)}{((350\,\text{mm})/2)}$$

$$= 47.2kNm$$

4. Determine the amplification factor, U_c.

$$U_c = \left(\frac{0.85}{1 - \frac{M_{fx}}{M_u}} \right)$$

$$= \left(\frac{0.85}{1 - \frac{(1733 kNm)}{(2532 kNm)}} \right)$$

$$= 2.694$$

5. Determine if the maximum calculated vertical moment, M_{fx}, has been reached.

$$\frac{M_{fx}}{M_r} + U_c \frac{w_c M_{fw}}{M_{ry}} \cong 1$$

$$\frac{(1733\ kNm)}{(2404\ kNm)} + (2.694) \frac{(0.5)(47.2\ kNm)}{(225.1\ kNm)} = 1.003 \cong 1$$

Therefore, the calculated moment resistance, M_{calc}, for the first-order, CSA S6-14 equation is 1733 kNm.

CSA S6-14 SECOND-ORDER ANALYSIS EQUATION

Sample calculation for model 075-8.33-100

Girder Dimensions:

b = 350 mm

t = 21 mm

h = 1000 mm

w = 13.3 mm

L = 8000 mm

R = 100 m

Girder Properties:

F_y = 350 MPa

E = 200 000 MPa

G = 77 000 MPa

Given:

M_y = 3280 kNm (from previous sample calculation)

M_r = 2404 kNm (from previous sample calculation)

M_u = 2532 kNm (from previous sample calculation)

CSA S6-14 Design Equation:

Determine the maximum calculated vertical moment, M_{fx}, that satisfies the equation shown below:

$$\frac{M_{fx}}{M_r} + U_c \frac{w_c M_{fw}}{M_{ry}} \leq 1$$

M_{fx} = vertical bending moment (from the 2nd order finite element model)

M_{fw} = lateral bending moment (from the 2nd order finite element model)

M_r = vertical bending moment resistance

= 2404 kNm (from previous sample calculation)

M_{ry} = lateral bending moment resistance

w_c = 0.5 for major lateral moment reversal between the lateral supports

U_c = 1.0 for second-order analyses

Calculations:

1. Determine the lateral bending moment resistance, M_{ry}. Note that for this analysis the applied lateral bending moment, M_{fw}, was calculated for a single flange only and neglected the contribution from the web. Therefore, the lateral bending moment resistance is calculated using only the single flange.

   Model 075-8.33-100 uses Class 2 flanges. Therefore, the lateral bending moment resistance is equivalent to the plastic moment of the rectangular shape.

$$M_{ry} = \frac{b^2 t F_y}{4}$$

$$= \frac{(350mm)^2 (21mm)(350MPa)}{4}$$

$$= 225.1kNm$$

2. Use the analysis output to determine if the maximum calculated vertical moment has been reached. The analysis provided output for every 1% increase in vertical moment. The output data from a specific increment step was used to determine if the maximum calculated vertical moment had been reached.

   When $M_{fx} = 1989kNm$, the following longitudinal stresses were in the compression flange tips at the midspan between lateral supports:

   σ_i = $382.5MPa$ in compression along the inside flange tip

   σ_o = $25.9MPa$ in compression along the outside flange tip

3. Determine the lateral bending moment, M_{fw}, from the stresses at the flange tips.

f_{bu} = vertical bending stress

$$= \left|\frac{\sigma_i + \sigma_o}{2}\right|$$

$$= \left|\frac{(-382.5MPa) + (-25.9MPa)}{2}\right|$$

$$= 204.2MPa$$

f_l = lateral bending stress

$$= f_{bu} - |\sigma_o|$$

$$= (204.2MPa) - |(-25.9MPa)|$$

$$= 178.3MPa$$

M_{fw} = $\dfrac{f_l\left(\dfrac{b^3 t}{12}\right)}{(b/2)}$ for a linear stress distribution

$$= \frac{(178.3MPa)\left(\dfrac{(350mm)^3(21mm)}{12}\right)}{((350\,\text{mm})/2)}$$

$$= 76.4kNm$$

4. Determine if the maximum calculated vertical moment, M_{fx}, has been reached.

$$\frac{M_{fx}}{M_r} + U_c \frac{w_c M_{fw}}{M_{ry}} \cong 1$$

$$\frac{(1989\ kNm)}{(2404\ kNm)} + (1.0)\frac{(0.5)(76.4\ kNm)}{(225.1\ kNm)} = 0.997 \cong 1$$

Therefore, the calculated moment resistance, M_{calc} for the second-order, CSA S6-14 equation is 1989 kNm.

AASHTO FIRST-ORDER ANALYSIS EQUATION

Sample calculation for model 075-8.33-100

Girder Dimensions:

b = 350 mm

t = 21 mm

h = 1000 mm

w = 13.3 mm

L = 8000 mm

R = 100 m

Girder Properties:

F_y = 350 MPa

E = 200 000 MPa

G = 77 000 MPa

I_x = 4.784×10^9 mm^4

I_y = 150.3×10^6 mm^4

C_w = 37.52×10^{12} mm^6

J = 2.945×10^6 mm^4

AASHTO Design Equation:

Determine the maximum calculated vertical moment, M_{fx}, that satisfies the equation shown below:

$$f_{bu} + A\frac{1}{3}f_l \le F_{nc}$$

f_{bu} = flange stress without considering lateral bending, or the vertical bending stress (from the 1st order finite element model)

f_l = flange lateral bending stress (from the 1st order finite element model)

F_{nc} = nominal flexural resistance of the flange

A = $\left(\frac{0.85}{1-\frac{f_{bu}}{F_{cr}}}\right)$ = amplification factor for first-order analyses

Calculations:

1. Determine F_{nc} based on the local buckling resistance and the lateral torsional buckling resistance of the equivalent straight member.

Local Buckling:

$$\lambda_f = \frac{b}{2t}$$

$$= \frac{(350mm)}{2(21mm)}$$

$$= 8.33$$

$$\lambda_{pf} = 0.38\sqrt{\frac{E}{F_y}}$$

$$= 0.38\sqrt{\frac{(200000MPa)}{(350MPa)}}$$

$$= 9.08$$

$\lambda_f \le \lambda_{pf} \therefore$

$$F_{nc} = R_b R_h F_y$$

$R_h = 1.0$ hybrid factor

$$R_b = 1 - \left(\frac{a_{wc}}{1200 + 300a_{wc}}\right)\left(\frac{h}{w} - \lambda_{rw}\right) \le 1.0$$

$$\lambda_{rw} = 5.7\sqrt{\frac{E}{F_y}}$$

$$= 5.7\sqrt{\frac{(200000MPa)}{(350MPa)}}$$

$$= 136$$

$$a_{wc} = \frac{hw}{bt}$$

$$= \frac{(1000mm)(13.3mm)}{(350mm)(21mm)}$$

$$= 1.810$$

$$R_b = 1-\left(\frac{(1.810)}{1200+300(1.810)}\right)\left(\frac{(1000mm)}{(13.3mm)}-(136)\right) \le 1.0$$

$$= 1.063 \ge 1.0 \therefore$$

$$= 1.0$$

$$F_{nc} = R_b R_h F_y$$

$$= (1.0)(1.0)(350\,\text{MPa})$$

$$= 350MPa$$

Therefore, $F_{nc} = 350MPa$ for the local flange buckling requirement. Now, check the lateral torsional buckling requirement.

Lateral Torsional Buckling:

$L = 8000mm$ unbraced length

$$L_p = 1.0 r_t \sqrt{\frac{E}{F_y}}$$

$$r_t = \frac{b}{\sqrt{12\left(1+\frac{1}{3}\frac{hw}{2bt}\right)}}$$

$$= \frac{(350mm)}{\sqrt{12\left(1+\frac{1}{3}\frac{(1000mm)(13.3mm)}{2(350mm)(21mm)}\right)}}$$

$$= 88.56mm$$

$$L_p = 1.0(88.56mm)\sqrt{\frac{(200000MPa)}{(350MPa)}}$$

$$= 2117mm$$

$$L_r = \pi r_t \sqrt{\frac{E}{F_{yr}}}$$

$$F_{yr} = 0.7F_y$$

$$= 0.7(350\,\text{MPa})$$

$$= 245MPa$$

$$L_r = \pi(88.56mm)\sqrt{\frac{(200000MPa)}{(245MPa)}}$$

$$= 7949mm$$

$L > L_r \therefore$

$$F_{nc} = F_{cr} \le R_b R_h F_y = 350MPa$$

$$F_{cr} = \frac{C_b R_b \pi^2 E}{\left(\frac{L}{r_t}\right)^2}$$

C_b = 1.0 for uniform bending moment

$$F_{cr} = \frac{(1.0)(1.0)\pi^2(200000MPa)}{\left(\frac{(8000mm)}{(88.56mm)}\right)^2}$$

$$= 241.9MPa$$

$F_{cr} \le 350MPa \therefore$

$$F_{nc} = 241.9MPa$$

Therefore, $F_{nc} = 241.9MPa$ for the lateral torsional buckling requirement.

Compare the nominal flexural resistance of the flange for local buckling $(F_{nc} = 350MPa)$ and lateral torsional buckling $(F_{nc} = 241.9MPa)$. The lowest value governs.

$\therefore F_{nc} = 241.9MPa$

2. Use the analysis output to determine if the maximum calculated vertical moment has been reached. The analysis provided output for every 1% increase in vertical moment. The output data from a specific increment step was used to determine if the maximum calculated vertical moment had been reached.

   When $M_{fx} = 1564kNm$, the following longitudinal stresses were in the compression flange tips at the midspan between lateral supports:

   σ_i = $259.6MPa$ in compression along the inside flange tip

   σ_o = $61.1MPa$ in compression along the outside flange tip

3. Determine the vertical bending stress, f_{bu}, from the stresses at the flange tips.

f_{bu} = vertical bending stress

$$= \left| \frac{\sigma_i + \sigma_o}{2} \right|$$

$$= \left| \frac{(-259.6MPa) + (-61.1MPa)}{2} \right|$$

$$= 160.3MPa$$

4. Determine the lateral bending stress, f_l, from the stresses at the flange tips.

f_l = lateral bending stress

$= f_{bu} - |\sigma_o|$

$= (160.3MPa) - |(-61.1MPa)|$

$= 99.2MPa$

5. Determine if the amplification factor, A, is required. If it is, calculate A.

If, $L \le 1.2L_p\sqrt{\frac{C_bR_b}{f_{bu}/F_y}}$, then amplifying the first-order lateral bending stress is not required.

$= 1.2L_p\sqrt{\frac{C_bR_b}{f_{bu}/F_y}}$

$= 1.2(2117mm)\sqrt{\frac{(1.0)(1.0)}{(160.3MPa)/(350\,\text{MPa})}}$

$= 3754mm$

$L = 8000mm > 3754mm \therefore$ Amplification of the lateral bending stress is required.

$A = \left(\frac{0.85}{1-\frac{f_{bu}}{F_{cr}}}\right) \ge 1.0$

$= \left(\frac{0.85}{1-\frac{(160.3MPa)}{(241.9MPa)}}\right) \ge 1.0$

$= 2.521 \ge 1.0$

$= 2.521$

6. Determine if the maximum calculated vertical moment, M_{fx}, has been reached.

$$f_{bu} + A\frac{1}{3}f_l \le F_{nc}$$

$$(160.3MPa) + (2.521)\frac{1}{3}(99.2MPa) \le (241.9MPa)$$

$$(243.7\ MPa) \cong (241.9\ MPa)$$

Therefore, the calculated moment resistance, M_{calc}, for the first-order, AASHTO equation is 1564 kNm.

AASHTO SECOND-ORDER ANALYSIS EQUATION

Sample calculation for model 075-8.33-100

Girder Dimensions:

b = 350 mm

t = 21 mm

h = 1000 mm

w = 13.3 mm

L = 8000 mm

R = 100 m

Girder Properties:

F_y = 350 MPa

E = 200 000 MPa

G = 77 000 MPa

I_x = 4.784×10^9 mm^4

I_y = 150.3×10^6 mm^4

C_w = 37.52×10^{12} mm^6

J = 2.945×10^6 mm^4

AASHTO Design Equation:

Determine the maximum calculated vertical moment, M_{fx}, that satisfies the equation shown below:

$$f_{bu} + A\frac{1}{3}f_l \le F_{nc}$$

f_{bu} = flange stress without considering lateral bending, or the vertical bending stress (from the 2nd order finite element model)

f_l = flange lateral bending stress (from the 2nd order finite element model)

F_{nc} = nominal flexural resistance of the flange

A = 1.0 when using a second-order analysis

Calculations:

1. Determine F_{nc} based on the local buckling resistance and the lateral torsional buckling resistance of the equivalent straight member.

Local Buckling:

$$\lambda_f = \frac{b}{2t}$$

$$= \frac{(350mm)}{2(21mm)}$$

$$= 8.33$$

$$\lambda_{pf} = 0.38\sqrt{\frac{E}{F_y}}$$

$$= 0.38\sqrt{\frac{(200000MPa)}{(350MPa)}}$$

$$= 9.08$$

$\lambda_f \le \lambda_{pf} \therefore$

$$F_{nc} = R_b R_h F_y$$

$R_h = 1.0$ hybrid factor

$$R_b = 1 - \left(\frac{a_{wc}}{1200 + 300a_{wc}}\right)\left(\frac{h}{w} - \lambda_{rw}\right) \le 1.0$$

$$\lambda_{rw} = 5.7\sqrt{\frac{E}{F_y}}$$

$$= 5.7\sqrt{\frac{(200000MPa)}{(350MPa)}}$$

$$= 136$$

$$a_{wc} = \frac{hw}{bt}$$

$$= \frac{(1000mm)(13.3mm)}{(350mm)(21mm)}$$

$$= 1.810$$

$$R_b = 1-\left(\frac{(1.810)}{1200+300(1.810)}\right)\left(\frac{(1000mm)}{(13.3mm)}-(136)\right) \le 1.0$$

$$= 1.063 \ge 1.0 \therefore$$

$$= 1.0$$

$$F_{nc} = R_b R_h F_y$$

$$= (1.0)(1.0)(350\,\text{MPa})$$

$$= 350MPa$$

Therefore, $F_{nc} = 350MPa$ for the local flange buckling requirement. Now, check the lateral torsional buckling requirement.

Lateral Torsional Buckling:

$L = 8000mm$ unbraced length

$$L_p = 1.0 r_t \sqrt{\frac{E}{F_y}}$$

$$r_t = \frac{b}{\sqrt{12\left(1+\frac{1}{3}\frac{hw}{2bt}\right)}}$$

$$= \frac{(350mm)}{\sqrt{12\left(1+\frac{1}{3}\frac{(1000mm)(13.3mm)}{2(350mm)(21mm)}\right)}}$$

$$= 88.56mm$$

$$L_p = 1.0(88.56mm)\sqrt{\frac{(200000MPa)}{(350MPa)}}$$

$$= 2117mm$$

$$L_r = \pi r_t \sqrt{\frac{E}{F_{yr}}}$$

$$F_{yr} = 0.7F_y$$

$$= 0.7(350\,\text{MPa})$$

$$= 245MPa$$

$$L_r = \pi(88.56mm)\sqrt{\frac{(200000MPa)}{(245MPa)}}$$

$$= 7949mm$$

$L > L_r \therefore$

$$F_{nc} = F_{cr} \le R_b R_h F_y = 350MPa$$

$$F_{cr} = \frac{C_b R_b \pi^2 E}{\left(\frac{L}{r_t}\right)^2}$$

C_b = 1.0 for uniform bending moment

$$F_{cr} = \frac{(1.0)(1.0)\pi^2(200000MPa)}{\left(\frac{(8000mm)}{(88.56mm)}\right)^2}$$

$$= 241.9MPa$$

$F_{cr} \le 350MPa \therefore$

$$F_{nc} = 241.9MPa$$

Therefore, $F_{nc} = 241.9MPa$ for the lateral torsional buckling requirement.

Compare the nominal flexural resistance of the flange for local buckling $(F_{nc} = 350MPa)$ and lateral torsional buckling $(F_{nc} = 241.9MPa)$. The lowest value governs.

$\therefore F_{nc} = 241.9MPa$

2. Use the analysis output to determine if the maximum calculated vertical moment has been reached. The analysis provided output for every 1% increase in vertical moment. The output data from a specific increment step was used to determine if the maximum calculated vertical moment had been reached.

   When $M_{fx} = 1818kNm$, the following longitudinal stresses were in the compression flange tips at the midspan between lateral supports:

   σ_i = $346.7MPa$ in compression along the inside flange tip

   σ_o = $26.5MPa$ in compression along the outside flange tip

3. Determine the vertical bending stress, f_{bu}, from the stresses at the flange tips.

f_{bu} = vertical bending stress

$$= \left| \frac{\sigma_i + \sigma_o}{2} \right|$$

$$= \left| \frac{(-346.7MPa) + (-26.5MPa)}{2} \right|$$

$$= 186.6MPa$$

4. Determine the lateral bending stress, f_l, from the stresses at the flange tips.

f_l = lateral bending stress

= $f_{bu} - |\sigma_o|$

= $(186.6MPa) - |(-26.5MPa)|$

= $160.1MPa$

5. Determine if the amplification factor, A, is required. If it is, calculate A.

Second-order analysis results were used, therefore, no amplification is required.

A = 1.0

6. Determine if the maximum calculated vertical moment, M_{fx}, has been reached.

$$f_{bu} + A\frac{1}{3}f_l \le F_{nc}$$

$$(186.6MPa) + (1.0)\frac{1}{3}(160.1MPa) \le (241.9MPa)$$

$(240.0\ MPa) \cong (241.9\ MPa)$

Therefore, the calculated moment resistance, M_{calc}, for the second-order, AASHTO equation is 1818 kNm.

CSA S6-06 FIRST-ORDER ANALYSIS EQUATION

Sample calculation for model 075-8.33-100

Girder Dimensions:

b = 350 mm

t = 21 mm

h = 1000 mm

w = 13.3 mm

L = 8000 mm

R = 100 m

Girder Properties:

F_y = 350 MPa

E = 200 000 MPa

G = 77 000 MPa

I_x = 4.784×10^9 mm^4

I_y = 150.3×10^6 mm^4

C_w = 37.52×10^{12} mm^6

J = 2.945×10^6 mm^4

S_x = 9.371×10^6 mm^3

CSA S6-06 Design Equation:

Determine the maximum calculated vertical moment, M_{fx}, that satisfies the equation shown below:

$$M_{fx} \leq M'_{rx}$$

M_{fx} = factored moment due to flexure (from the 1st order finite element model)

M'_{rx} = modified buckling moment that includes the effects of curvature

Calculations:

1. Use the analysis output to determine if the maximum calculated vertical moment has been reached. The analysis provided output for every 1% increase in vertical moment. The output data from a specific increment step was used to determine if the maximum calculated vertical moment had been reached.

   When $M_{fx} = 1057 kNm$, the following longitudinal stresses were in the compression flange tips at the midspan between lateral supports:

   σ_i = $175.4 MPa$ in compression along the inside flange tip

   σ_o = $41.3 MPa$ in compression along the outside flange tip

2. Determine the modified buckling moment, M'_{rx}.

$$M'_{rx} = F_y S_x \left(1 - 3\lambda^2\right) \rho_b \rho_w$$

$$\lambda = \frac{L}{2b}\sqrt{\frac{F_y}{\pi^2 E}}$$

$$= \frac{(8000mm)}{2(350mm)}\sqrt{\frac{(350MPa)}{\pi^2 (200000MPa)}}$$

$$= 0.152$$

$$\rho_b = \frac{1}{1 + \left(\frac{L}{R}\right)\left(\frac{L}{2b}\right)}$$

$$= \frac{1}{1 + \left(\frac{(8000mm)}{(100000mm)}\right)\left(\frac{(8000mm)}{2(350mm)}\right)}$$

$$= 0.522$$

ρ_w = Because f_w is in tension on the outside edge, therefore $\frac{f_w}{f_b}$ is negative,

therefore $\rho_w = \rho_{w1}$

$$\rho_{w1} = \frac{1}{1-\frac{f_w}{f_b}\left[1-\frac{L}{150b}\right]}$$

f_b = flexural stress

$$= \left|\frac{\sigma_i + \sigma_o}{2}\right|$$

$$= \left|\frac{(-175.4MPa)+(-41.3MPa)}{2}\right|$$

$$= 108.3MPa$$

f_l = warping normal stress

$$= \sigma_i + f_b$$

$$= (-175.4MPa)+(108.3MPa)$$

$$= -67.1MPa$$

$$\rho_{w1} = \frac{1}{1-\frac{(-67.1MPa)}{(108.3MPa)}\left[1-\frac{(8000mm)}{150(350mm)}\right]}$$

$$= 0.656$$

$$M_{rx}^{'} = (350MPa)(9.371\text{x}10^6\ \text{mm}^3)\left(1-3(0.152)^2\right)(0.522)(0.656)$$

$$= 1046kNm$$

3. Check if $M_{fx} \cong M_{rx}^{'}$.

$M_{fx}=1057kNm \cong M_{rx}^{'}=1046kNm$

Therefore, the calculated moment resistance, M_{calc}, for the first-order, CSA S6-06 equation is 1057 kNm.

CSA S6-06 SECOND-ORDER ANALYSIS EQUATION

Sample calculation for model 075-8.33-100

Girder Dimensions:

b = 350 mm

t = 21 mm

h = 1000 mm

w = 13.3 mm

L = 8000 mm

R = 100 m

Girder Properties:

F_y = 350 MPa

E = 200 000 MPa

G = 77 000 MPa

I_x = 4.784×10^9 mm^4

I_y = 150.3×10^6 mm^4

C_w = 37.52×10^{12} mm^6

J = 2.945×10^6 mm^4

S_x = 9.371×10^6 mm^3

CSA S6-06 Design Equation:

Determine the maximum calculated vertical moment, M_{fx}, that satisfies the equation shown below:

$$M_{fx} \leq M'_{rx}$$

M_{fx} = factored moment due to flexure (from the 2nd order finite element model)

M'_{rx} = modified buckling moment that includes the effects of curvature

Calculations:

1. Use the analysis output to determine if the maximum calculated vertical moment has been reached. The analysis provided output for every 1% increase in vertical moment. The output data from a specific increment step was used to determine if the maximum calculated vertical moment had been reached.

   When $M_{fx} = 991 kNm$, the following longitudinal stresses were in the compression flange tips at the midspan between lateral supports:

   σ_i = $174.7 MPa$ in compression along the inside flange tip

   σ_o = $28.6 MPa$ in compression along the outside flange tip

2. Determine the modified buckling moment, M'_{rx}.

$$M'_{rx} = F_y S_x \left(1 - 3\lambda^2\right) \rho_b \rho_w$$

$$\lambda = \frac{L}{2b}\sqrt{\frac{F_y}{\pi^2 E}}$$

$$= \frac{(8000mm)}{2(350mm)}\sqrt{\frac{(350MPa)}{\pi^2 (200000MPa)}}$$

$$= 0.152$$

$$\rho_b = \frac{1}{1 + \left(\frac{L}{R}\right)\left(\frac{L}{2b}\right)}$$

$$= \frac{1}{1 + \left(\frac{(8000mm)}{(100000mm)}\right)\left(\frac{(8000mm)}{2(350mm)}\right)}$$

$$= 0.522$$

ρ_w = Because f_w is in tensiona on the outside edge, therefore $\frac{f_w}{f_b}$ is negative,

therefore $\rho_w = \rho_{w1}$

$$\rho_{w1} = \frac{1}{1-\frac{f_w}{f_b}\left[1-\frac{L}{150b}\right]}$$

f_b = flexural stress

$$= \left|\frac{\sigma_i + \sigma_o}{2}\right|$$

$$= \left|\frac{(-174.7MPa)+(-28.6MPa)}{2}\right|$$

$$= 101.6MPa$$

f_l = warping normal stress

$$= \sigma_i + f_b$$

$$= (-174.7MPa)+(101.6MPa)$$

$$= -73.0MPa$$

$$\rho_{w1} = \frac{1}{1-\frac{(-73.0MPa)}{(101.6MPa)}\left[1-\frac{(8000mm)}{150(350mm)}\right]}$$

$$= 0.621$$

$$M'_{rx} = (350MPa)(9.371\text{x}10^6\ \text{mm}^3)\left(1-3(0.152)^2\right)(0.522)(0.621)$$

$$= 991kNm$$

3. Check if $M_{fx} \cong M'_{rx}$.

$M_{fx}=991kNm \cong M'_{rx}=991kNm$

Therefore, the calculated moment resistance, M_{calc}, for the second-order, CSA S6-06 equation is 991 kNm.